DESIGN OF A SUPERSONIC SHOCK TUNNEL AND EXPERIMENTAL SURFACE MEASUREMENTS

by

YAGNAVALKYA S. MUKKAMALA

Thesis submitted to the faculty of the

Virginia Polytechnic Institute and State University

in partial fulfillment of the requirements for the degree of

MASTER OF SCIENCE

in

Mechanical Engineering

APPROVED:

Thomas E. Diller, Chairman

Alfred L. Wicks

Joseph A. Schetz

May, 1993

Blacksburg, Virginia

DESIGN OF A SUPERSONIC SHOCK TUNNEL AND EXPERIMENTAL SURFACE MEASUREMENTS

by

Yagnavalkya S. Mukkamala

Committee Chairman: Thomas E. Diller

Mechanical Engineering

Abstract

The design, development, construction, and instrumentation features of a supersonic shock tunnel that produced high temperature supersonic flow for a short duration, on the order of 2 msec, are presented. The shock tunnel was equipped with a Mach 3 supersonic 2-D nozzle. Test runs were conducted using air and helium drivers at driving pressures varying from 200-450 psig (1.4-3.1 MPa gage), with the driven gas in all the cases being ambient air. Pressure and temperature measurements were made to document the operating conditions of the tunnel. Total pressure measurements were made in the settling chamber of the nozzle where the flow Mach number is 0.14 (weakly subsonic). Static pressure measurements were made at the exit of the nozzle to establish the unsteady starting process of the nozzle. Total temperature measurements using thermocouples were made in the settling chamber of the nozzle to identify the maximum

temperature attained in the flow. Surface heat flux measurements were made at the exit of the nozzle and compared with previous skin friction measurements.

The measured pressures and temperatures compared well with the predicted values for the air driver. In the case of the test runs with the helium driver the nozzle started, but the flow was unsteady. Consequently, there were difficulties in making measurements and interpreting them. The surface heat flux and skin friction followed the Reynold's analogy within 50% during the steady run time of the shock tunnel.

ACKNOWLEDGEMENTS

Firstly, I would like to express my humble thanks to GOD almighty, and his son Jesus Christ in whom I abide forever. The constant support of my brothers and sisters at Slussers Chapel has indeed been a divine blessing. Utmost respects are due to my parents for helping me dream big.

I also express my sincerest thanks and gratitude to my advisor Prof. Diller who was extremely patient with me throughout this endeavor and helped me in every conceivable way. He is responsible for whatever modest skills I developed during the undertaking of this research.

I also thank Prof. Schetz for his continuous involvement with this project and his innumerable suggestions. His help particularly concerning the fluid dynamics aspect of this research is much appreciated.

I wish to thank Prof. Wicks for his encouragement and often outright humor filled suggestions concerning data acquisition and instrumentation that made me realize that graduate research can be enjoyable.

I would like to thank Prof.Moore for his "outside" involvement with my research. His encouragement is much appreciated.

I can't but emphasize the significance of the help rendered to me by the technicians of the Mechanical Engineering shop, particularly Johnny Cox, Jerry Lucas, Red Fisher, Randall Smith, and Billy Shepherd. Thanks is also extended to the technicians of the AOE shop, Frank Shelor and Kent Morris.

Finally I would like to thank all my friends, Dr.K.M.Chadwick, Dr.R.Bowersox, Dr.D.J.Deturris, Michael Novean, Brice Lancon, Roger Doughty, John Busic, Steve Horvath, Brian Kafka and Brian Lattimer for their individual assistance for this project.

This is not the presentation of a perfect work, for I have committed many a mistake before learning anything the right way. But, I do hope that GOD ALMIGHTY still recognizes the effort, for everything I do is to glorify HIS blessed name.

TABLE OF CONTENTS

LIST OF FIGURES

LIST OF SYMBOLS

A	Area of Cross-Section
A_{sur}	Surface Area
A^*	Area of Cross-Section of the Throat
a	Sound Speed
C_f	Coefficient of Skin Friction
C_p	Specific Heat
D	Diameter
h	Convective Heat Transfer Coefficient
K	Thermal Conductivity
m	Mass
M	Mach Number
Nu	Nusselt Number
p	Pressure
Pr	Prandtl Number
q''	Surface Heat Flux
r	Recovery Factor
Re	Reynolds Number
St	Stanton number
t	Time

T	Temperature
u	Gas Speed
V	Velocity
W	Speed of a Shock Wave
y	Coordinate
γ	Specific Heat Ratio
ρ	Density
μ	Absolute Viscosity
χ_1	Length of the Driven Section
χ_4	Length of the Driving Section
τ	Thermocouple Time Constant
τ_w	Wall Shear Stress
$\Delta\tau$	Incident Shock Run Time
Δ_r	Reflected Shock Run Time

Subscripts

0	Stagnation Property
1	Conditions Upstream of a Shock Wave
2	Conditions Downstream of a Shock Wave
3	Conditions Upstream of the Contact Surface
4	Initial Conditions of the Driven Gas
5	Conditions Downstream of the Reflected Shock Wave

avg	Average Property
aw	Adiabatic Wall Conditions
D	Property Based on the Diameter
R	Property of the Reflected Shock Wave
s	Incident Shock Conditions
w	Property Evaluated At The Wall
∞	Free-Stream Conditions

CHAPTER 1

INTRODUCTION

1.1 OBJECTIVE

The purpose of the presented research was to design and construct a shock tunnel that produced high enthalpy supersonic flow for at least 2 milliseconds. This was necessary to test the time response of the skin friction sensors. The shock tunnel was also intended to be used for studying the response of the Heat Flux Microsensor.

1.2 MOTIVATION

As part of the NASP project, work is currently being done on gaining a better understanding of the nature and magnitude of frictional head losses in **supersonic combustion ramjet engines**. Skin friction balances have been designed and instrumented to measure the wall shear stress and thus the associated skin friction coefficient. Measurement of the frictional drag and the associated pressure loss provides an understanding of the overall combustor efficiency and thrust losses. Wall shear stress in supersonic flows with combustion was observed to increase with the onset of combustion. In order to effectively utilize these skin friction balances in such conditions

it became important to have access to a test facility that produced high enthalpy supersonic flow. The construction of a steady, long run facility operating at these conditions necessitates extensive cooling systems to remove the large quantities of heat produced during the combustion process. Needless to say this is a very expensive and complex undertaking. Shock tunnels, which are also known as impulse tunnels, utilize the phenomenon of the abrupt increase in the temperature and pressure across a traveling shock wave to produce high temperature and pressure conditions. These conditions, however, exist only for a fraction of a second. The skin friction sensors need to have a very high natural frequency, with a typical response time of less than one msec. To validate and establish the projected response times of these sensors, it was decided to construct an impulse facility that would produce supersonic flow for a short duration.

CHAPTER 2

BACKGROUND

2.1 BASIC SHOCK TUBE AND SHOCK TUNNEL: DIFFERENT TYPES

A shock tube is composed of a long pipe divided into two sections. The shorter section called the driving section is filled with a pressurized gas and the longer section called the driven section is either left open to the atmosphere or is evacuated to lower pressures. Sometimes, the driven section is filled with a low pressure gas. The two sections are separated by a diaphragm that is usually made of metal or plastic.

A shock tunnel is a shock tube with a nozzle attached to its end. This nozzle is used to accelerate the gas flow to supersonic speeds. Depending upon the situation the nozzle is either a converging-diverging nozzle or a diverging nozzle. The resulting shock tunnel is either a "Reflected shock tunnel" or an "Incident shock tunnel". A reflected shock tunnel has a converging-diverging nozzle attached to it. The throat of such a nozzle is very small when compared to the cross-section of the tube, and hence most of the incident shock wave is reflected back into the shock tube. This reflected shock wave produces a region of almost stagnant high pressure gas. This compressed gas then acts as a reservoir for the nozzle. A non-reflected shock tunnel, however,

utilizes either a diverging nozzle or a transition nozzle. In this case the traveling shock wave is just transmitted through and the gas behind it (which travels at low supersonic speeds) is expanded to much higher supersonic speeds or hypersonic speeds in the diverging nozzle.

Shock tunnels also differ in the type of driving technique that they employ. Some of the most common driving techniques are combustion drivers, arc ignited drivers, explosive drivers, electromagnetic drivers, piston drivers, implosion drivers, etc. The main purpose of any driving technique is to produce the appropriate pressure and temperature conditions(both stagnant and flow values), while at the same time resulting in a fairly uniform and steady flow for an appreciable run time. The NASA Ames research center, for example, has an operational high-explosive shock tunnel. This tunnel is a shock tube utilizing one single gas that is compressed by a glass piston which is propelled by an explosive. There are also facilities that heat the driving gas using electric arcs. A hot driving gas results in a stronger shock and higher total temperature and pressure conditions in the nozzle. Hence the driving technique involved can make a lot of difference in the performance of a shock tunnel. Further description regarding basic shock tubes and their classification is given by Gaydon (1963).

2.2 UTILITY OF SHOCK TUNNELS/TUBES

The following shock tunnel applications have been elaborated upon by Gaydon(1963). Shock tunnel or shock tube research falls under two basic categories:

(1) Applied aerodynamics/fluid dynamics research and (2) Applied physical research

2.2.a APPLIED AERODYNAMICS/FLUID DYNAMICS RESEARCH

Shock tunnels are used to simulate the stagnation enthalpy and pressure of hypersonic flight conditions. Sustaining such conditions for a long duration may be extremely difficult if not impossible by using steady facilities, like wind tunnels. Aerodynamic applications also include the study of heat transfer, ablation, free-stream turbulence and wall shear stress and dynamic frictional pressure losses at hypersonic speeds. Shock tunnels are used, for example in the NASP project, to simulate the supersonic combustion conditions encountered in the supersonic combustors. Shock tunnels are capable of housing scaled SCRAMJET models, and thus facilitate the study of the dynamic response of these models to hypersonic flows over them. These are but a few of the many high speed fluid dynamics applications for shock tunnels.

2.2.b APPLIED PHYSICAL RESEARCH

Applications in chemistry include the study of combustion processes and mixed gas reactions, study of the emission and absorption spectra of the compressed, ionized high temperature gases. Applications also include the study of reaction rates and ionization rates in chemical kinetics. Physical chemistry applications include the study of different modes of energy storage and transmission in gas molecules(like translation, rotation, and vibration), study of molecular relaxation times, and also study of electronic

excitation and attendant spectral radiation. Astrophysical applications include using the shock tube to produce an ionized gas state, and to compare the radiation from the ionized molecules with the stellar radiation of a particular star. Such comparisons lead to both qualitative and quantitative estimates for the atmospheric conditions of stars.

2.3 REVIEW OF SHOCK TUNNEL RESEARCH

Gaydon (1963) presents an extensive coverage on the various aspects of the construction of a shock tunnel. This was used as the primary reference for the design features of the shock tunnel. Flow measurements similar to those made in the half nozzle were conducted by Witliff et al. (1958) during their research on a tailored interface hypersonic shock tunnel. This Cornell facility utilizes special driving conditions to eliminate the reflection of the shock wave from the contact surface, thereby producing a much longer steady-flow test time. They have also conducted heat flux measurements on a hemisphere model. Extensive research has been done on the construction and usage of shock tunnels for aerodynamic research and for making surface measurements. General Applied Science Laboratory, has a 3 inch diameter valve-actuated shock tube. They use it for general aerospace research and for studying the heat transfer in short duration test times. The researchers at GASL conducted studies on the phenomenon of shock attenuation and boundary layer growth behind the traveling incident shock wave. Their research was the motivation behind the analysis of shock strengths presented in chapter 6. Amman et al. (1973) have investigated the starting process of a shock tunnel

nozzle and established the approximate starting time. This paper partially assisted in understanding the concept of the starting of the Mach 3 half nozzle attached to the supersonic shock tunnel.

CHAPTER 3

FLOW FIELD IN A SHOCK TUNNEL

3.1 BASIC WAVE FORMATION AND PROPAGATION IN A SHOCK TUNNEL

This section focusses on the description of various kinds of waves formed in a shock tunnel. The following ideas regarding wave formation and propagation are due to Gaydon (1963).

3.1.1 GENERATION OF A SHOCK WAVE: As portrayed in Fig. 1, the driving section of the shock tube or tunnel is pressurized with the appropriate driving gas, while the driven section is either filled with the appropriate driven gas at the corresponding pressure, or left open to the atmosphere. Figure shows the shock formation process. When the diaphragm between the driver and driven sections is ruptured, the high pressure driving gas expands into the low pressure driven section of the tube. This sudden expansion produces finite compression waves, which as shown in the Fig. 2, are right running C_+ characteristics. Each of these compression waves travels with speed, u+a, where u is the local wave velocity and a the local sound speed. Every finite traveling wave induces a mass motion in the gas behind it. Since a compression wave

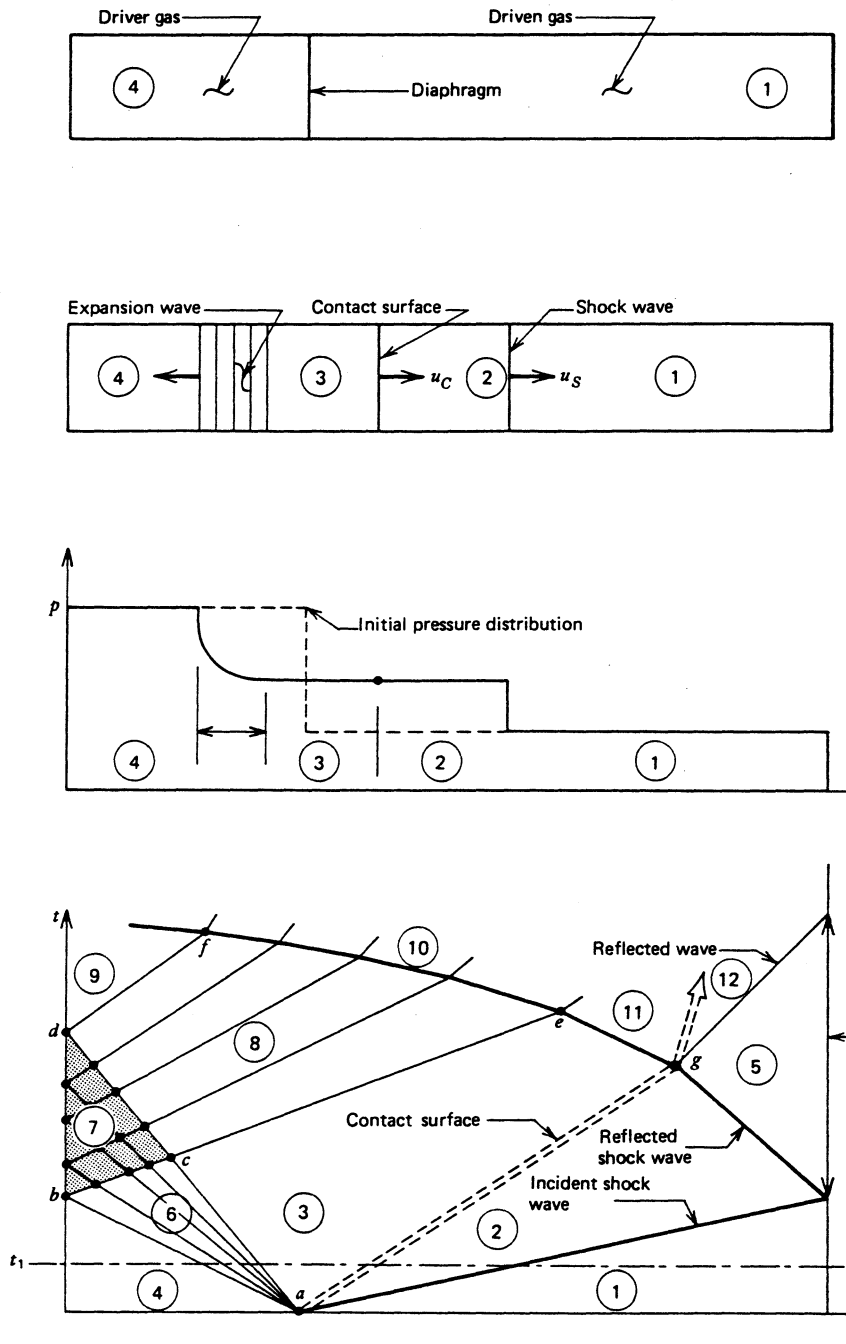

Figure 1 : Simple Shock Tube and the Wave Pattern (Gaydon et al., 1963)

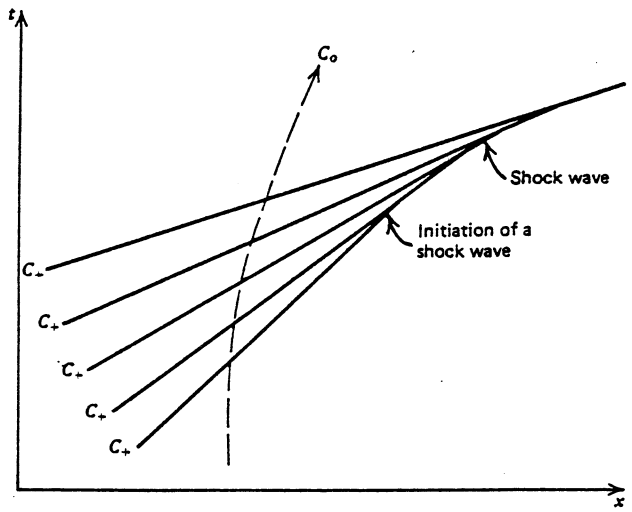

Figure 2 : Formation of a Shock Wave (Zucrow et al.)

increases the pressure, temperature and hence the sound speed, every finite compression wave travels at a speed greater than the speed of its preceding counterpart. Eventually all these compression waves coalesce into a shock wave. The point at which these waves start coalescing is called the shock initiation point.

Theoretically the formation of this shock wave can be considered to be instantaneous. This shock formation process can take a finite amount of time, the equivalent distance of several tube diameters. It has been observed that this distance increases with increasing shock Mach numbers, and that it is greater for helium driver than for hydrogen driver. This is because in the case of a combustion driver like hydrogen, the sound speed is larger, and hence the Mach number is lower for the same test conditions. A big shock Mach number is a result of faster compression waves, which in turn lower the shock formation distance and time. The diaphragm opening process has considerable impact on the shock formation process. The diaphragm opening takes several hundred microseconds. During this time the flow is extremely unsteady and three dimensional in nature. The shock wave forms over a finite tube length and accelerates to its maximum design Mach number.

3.1.2 CONTACT SURFACE: The contact surface is a contact discontinuity or interface that separates two zones of gases at different temperatures. Once the shock wave starts traveling down the driven section it induces a mass motion in the gas behind it. This gas, which is also known as the shocked gas, is compressed and is at a temperature that

is higher than that of the unshocked driven gas. The contact surface thus separates this shock compressed driven gas from the quiescent driven gas. The pressure and the gas velocity across the contact surface are conserved. In fact the contact surface replaces the diaphragm, once it ruptures, as the separation between the driving gas and the driven gas.

The contact surface travels in the same direction as the shock wave, and with the same velocity as that of the shock compressed gas. This is evident from Fig. 1, where the velocities of both the contact surface and the gas in region 2, are u_2. Theoretically, the contact surface is viewed as an infinitely thin interface. However, it is a zone of finite thickness involving the turbulent mixing of the driving and driven gases.

3.1.3 EXPANSION WAVES: In order to maintain the equilibrium of pressure, a shock wave is generated and propagated into the low pressure section increasing the pressure of the driven gas. At the same time an expansion fan is generated and propagated into the driving gas reducing its pressure. Both sets of waves are generated at the diaphragm station, once the diaphragm ruptures. The expansion fan is a set of isentropic rarefaction waves, the expansion head leading the fan with the expansion tail, trailing. This unsteady expansion fan is in many ways similar to the steady, planar centered Prandtl-Meyer expansion fan. The entropy is conserved across the expansion fan. However, the pressure drops in the gas behind the fan (that is in region 3 in Fig. 1).

The head of the expansion fan travels into the still driving gas with the local

sound speed a_4, where zone 4, as depicted in Fig. 1, is the driving gas zone. Every subsequent wave in this expansion fan travels at a speed u-a, where a and u are the local sound speed and velocity of the induced mass motion in the driving gas (which is in the same direction as the travel of the contact surface). The head of this expansion fan propagates into the still driving gas. This centered expansion fan is isentropic. The local temperature and hence sound speed behind the successive waves decreases in magnitude. Thus the head of the expansion fan travels with the largest speed (a_4, direction to the left in Fig. 1) with every successive wave in the fan traveling at a lower velocity. In fact, for the case of very weak shock waves, the tail of the expansion fan may completely switch directions and travel in the same direction as that of the shock wave.

3.2 STARTING OF AN UNSTEADY NOZZLE

The intention in including this topic is to emphasize the complex nature of transmission and reflection of waves during the starting process of an unsteady nozzle, for example a shock tunnel nozzle. Without a fundamental knowledge of the mechanism of shock wave and rarefaction wave formation and propagation during this starting period, it is very difficult to understand some of the trends in the measured pressure and other data traces. A more detailed analysis regarding the nature of the wave propagation and interactions is presented by Shapiro (1953,1954) and Gaydon (1963).

There are essentially two conditions that have to be met for an unsteady nozzle to start. One of them is that the plenum or reservoir pressure has to reach the required

value. The other is that all of the unsteady waves resulting from the shock wave formation and other wave interactions in the driven section, have to pass through the nozzle before equilibrium conditions can be established.

Initially the incident shock wave traveling down the driven section encounters a sudden area change when it is at the nozzle inlet. This shock wave is then partially transmitted into the nozzle and partially reflected back into the driven section. A contact discontinuity is then formed at the nozzle inlet. If the nozzle is a converging-diverging nozzle, then the shock wave will encounter a second area change at the throat. Once again the shock wave is partially transmitted downstream and partially reflected upstream, with a contact surface being formed at the throat. As this shock wave is transmitted into the nozzle, Mach reflections off the wall of the nozzle produce a secondary shock wave that travels behind the primary transmitted shock wave. This shock wave is preceded by a region of decreasing gas velocity behind the primary transmitted shock wave, and is succeeded by a region of growing supersonic velocity downstream of the throat. All of these waves have to completely pass through, before the nozzle can start. This while the pressure in the plenum is at the appropriate value to produce supersonic flow in the nozzle. Consequently, there is a finite starting time for an unsteady nozzle. This is obviously a disadvantage because the plenum pressure will not stay constant until the nozzle starts if the contact surface reaches the plenum before the nozzle starts.

In Fig. 3 are included a series of shadow graphs taken by Amman et al. (1973)

at different instances in time for a reflected nozzle, which illustrate the starting process of an unsteady reflected nozzle with a rounded end based on the principles discussed in the previous paragraph. The incident shock Mach number is 3.0 and the time intervals between these pictures (from top to bottom) is 35, 50 and 190 μsec respectively. Figure 3a depicts the arrival of the incident shock wave at the throat of this reflected nozzle and its subsequent transmission into the nozzle. In Fig. 3b the formation of the secondary shock wave due to the reflections off the nozzle's wall is clear. Also from this figure is the formation of a contact surface and distinct vortices behind the transmitted incident shock wave. Figure 3c shows the travel of these unsteady waves down the nozzle. Supersonic flow can't be produced in the nozzle until all these unsteady waves are transmitted completely through the nozzle. This is evident from Fig. 3d where all these waves pass through and the nozzle finally starts, producing supersonic flow.

3.3 DEVIATIONS FROM IDEALISTIC CONDITIONS

The theoretical run time and flow properties are the ideal counterparts of the measured values. The most common deviations from the ideal parameters are due to the viscous and real gas effects of gas flow in ducts. As the shock wave travels down the driven section of the tunnel, the viscosity of the driven gas slows down the fluid adjacent to the wall, forming a boundary layer. The fluid in this boundary layer travels at a much lower velocity than that in the inviscid central core, which travels at velocity u_2, the velocity of induced mass motion behind the shock wave. This boundary layer reduces

Attention Patron:

Page 16 omitted from numbering

the effective mass flow in the central core, and thus can have a profound impact on the run time (can decrease it by about 50%), and other flow properties.

Figure 4 depicts the process of the development and growth of the boundary layer in a shock tube. The boundary layer starts growing behind the traveling shock wave. It has zero thickness at the shock wave and the expansion head. This boundary layer consists of a mixture of driving and driven gases. All the viscous and heat transfer effects are confined to within the boundary layer. The velocity gradients are concentrated in the hydrodynamic boundary layer. The temperature gradients, and heat transfer, are concentrated in the thermal boundary layer. Detailed analysis of the shear stress measurements is presented in chapter 8. A more detailed discussion regarding the viscous effects of the boundary layer on the shock formation and propagation process, and the flow properties is presented by Gaydon (1963).

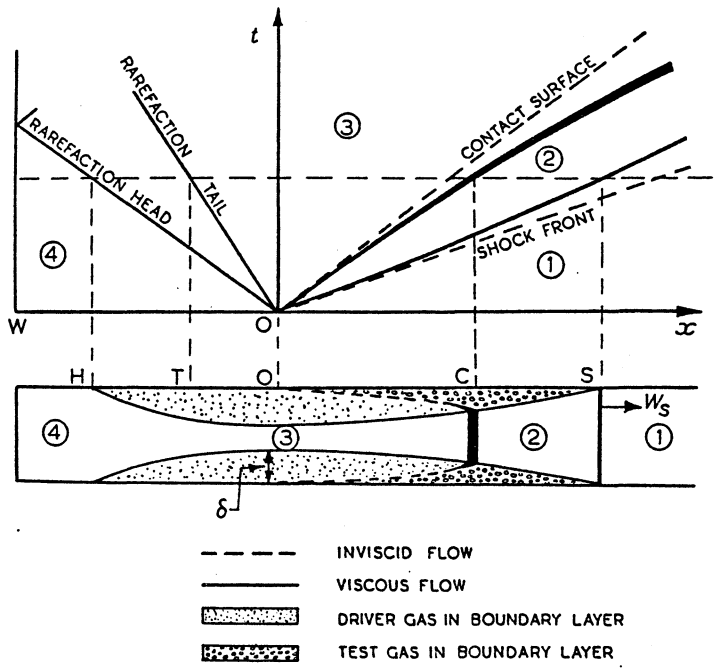

Figure 4 : Boundary Layer Growth in a Shock Tube (Gaydon et al., 1963)

CHAPTER 4

BASIC DESIGN ATTRIBUTES OF A SHOCK TUNNEL

The design features of a typical supersonic shock tunnel that can be used for experimental research in high speed fluid dynamics, are discussed below. The equations listed are referenced from Gaydon (1963) and Anderson (1990).

4.1 DESIRED RUN TIME

The run time is defined as the duration during which the flow is steady and fairly uniform. There are two types of run times: an incident shock run time and a reflected shock run time. The run time in the case of an incident shock tunnel is the duration between the arrival of the incident shock wave at the nozzle inlet and the arrival of the unsteady interface, the contact surface. The incident shock run time is calculated by using equation

$$\Delta\tau = \tau_c \left[1 - \frac{2\left(M_s^2 - 1\right)}{\left(\gamma_1 + 1\right) M_s^2} \right] \qquad (1)$$

where M_s is the incident shock Mach number. In Eq. 1 τ_c is the time it takes for the reflected rarefaction head of the expansion fan to catch up with the contact surface. It

is given by the expression

$$\tau_c = \frac{2\chi_4}{a_4}\left[1 - \frac{\gamma_4 - 1}{\gamma_1 + 1}\frac{a_1}{a_4}\left(\frac{M_s^2 - 1}{M_s^2}\right)\right]^{-\left(\frac{\gamma_4+1}{2(\gamma_4-1)}\right)} \qquad (2)$$

in which, χ_4 is the length of the driving section of the shock tunnel. γ_4 and γ_1 are the specific heat ratios of the driving and driven gases, while a_4 and a_1 are the sound speeds in the driving and driven gases at their ambient temperatures.

The run time for a reflected shock tunnel is the time lag between the arrival of the incident shock wave at the wall or the nozzle inlet (as the case may be) and the arrival of the re-reflected wave that bounces off the contact surface after the reflected shock wave (reflected off the wall) hits the contact surface. The arrival of the contact surface marks the onset of non-uniform, unsteady flow. This run time is usually $2\Delta\tau_r$ or $3\Delta\tau_r$ (Gaydon 1963) where τ_r is the time it takes for the reflected shock wave to reach the contact surface and is given by the equation

$$\Delta\tau_r = \frac{\chi_1}{W_S}\left(\frac{W_S - u_2}{W_R + u_2}\right) \qquad (3)$$

The parameters W_S, W_R which are the incident shock and reflected shock speeds are calculated using equations

$$W_s = a_1 \sqrt{\frac{\gamma+1}{2\gamma}\left[\frac{p_2}{p_1}-1\right]+1} \tag{4}$$

$$\frac{W_R}{W_S} = \frac{2+\frac{2}{\gamma-1}\frac{p_1}{p_2}}{\frac{\gamma+1}{\gamma-1}-\frac{p_1}{p_2}} \tag{5}$$

In Eq. 4 and Eq. 5 p_1 and p_2 are the pressures downstream and upstream of the traveling incident shock wave, while γ is the specific heat ratio of the driven gas.

The induced mass motion velocity behind the traveling incident shock wave, u_2 is

$$u_2 = \frac{a_1}{\gamma}\left[\frac{p_2}{p_1}-1\right]\left[\frac{\frac{2\gamma}{\gamma+1}}{\frac{p_2}{p_1}+\frac{\gamma-1}{\gamma+1}}\right] \tag{6}$$

The pressure ratio across the traveling incident shock wave is

$$\frac{p_2}{p_1} = 1+\frac{2\gamma}{\gamma+1}(M_s^2-1) \tag{7}$$

The temperature ratio across the traveling shock wave is

$$\frac{T_2}{T_1}=\frac{p_2}{p_1}\left[\frac{\frac{\gamma+1}{\gamma-1}+\frac{p_2}{p_1}}{1+\frac{\gamma+1}{\gamma-1}\frac{p_2}{p_1}}\right] \tag{8}$$

4.2 DESIRED STAGNATION AND FLOW PROPERTIES

The desired stagnation temperature and pressure conditions depend upon the particular operation for which the shock tunnel was built. For example, shock tunnels used for high temperature chemical kinetics research in compressed ionized gases run at very high enthalpy conditions with high stagnation temperatures. Conversely, shock tunnels with attached hypersonic nozzles, which are utilized for high speed aerodynamics research requiring the acceleration of the flow to hypersonic speeds, operate at very high total pressure conditions. Hence, the particular operation of the shock tunnel dictates the relevant flow conditions like total pressure, total temperature, flow Mach number, and run time.

The stagnation conditions in the case of an incident shock tunnel are given by the standard isentropic compressible fluid relations

$$p_0=p\left[1+\frac{\gamma-1}{2}M^2\right]^{\frac{\gamma}{\gamma-1}} \tag{9}$$

$$T_0 = T\left[1+\frac{\gamma-1}{2}M^2\right] \tag{10}$$

In the case of a reflected shock tunnel, the stagnation properties are those behind the reflected shock wave. Equations 11 and 12 are due to Gaydon et al. (1963).

$$p_5 = p_1\left[\frac{2\gamma M_s^2-(\gamma-1)}{\gamma+1}\right]\left[\frac{(3\gamma-1)M_s^2-2(\gamma-1)}{(\gamma-1)M_s^2+2}\right] \tag{11}$$

$$T_5 = T_1\frac{\left(2(\gamma-1)M_s^2+(3-\gamma)\right)\left((3\gamma-1)M_s^2-2(\gamma-1)\right)}{(\gamma+1)^2 M_s^2} \tag{12}$$

4.3 CHOICE OF TEST GASES AND GAS PRESSURES

The next stage in this design process is the selection of the appropriate test and driving gas pressures. For identical test conditions, a lighter driving gas driving a heavier driven gas produces a stronger and faster shock with larger stagnation conditions than a heavier driving gas driving the same driven gas. The total pressure required in a shock tunnel is dependent on the desired flow Mach number. In the case of a reflected shock tunnel the stagnation pressure is the pressure of the stagnant gas behind the reflected shock wave, which, neglecting losses, is the same as the total pressure in the flow. In an incident shock tunnel this pressure is the total pressure of the shocked gas

in the zone between the incident shock wave and the traveling contact surface. So in both the cases the total pressure is directly proportional to the shock strength, which is a function of its Mach number. Further, the flow Mach number is related to the desired run time. Also, the shock strength is directly related to the pressure ratio of the driving and driven gases, or the diaphragm pressure ratio. So the flow parameters pre-specify the diaphragm pressure ratio. Once the driven gas pressure is known, the driving gas pressure can then be calculated from the diaphragm pressure ratio. The diaphragm pressure ratio, which is the ratio of the driving and driven gas pressures is given by equation

$$\frac{p_4}{p_1} = \frac{2\gamma_1 M_s^2 - (\gamma_1 - 1)}{\gamma_1 + 1} \left[1 - \frac{\gamma_4 - 1}{\gamma_1 + 1} \frac{a_1}{a_4} \left(M_s - \frac{1}{M_s} \right) \right] \left[-\frac{2\gamma_4}{\gamma_4 - 1} \right] \qquad (13)$$

where p_4 and p_1 are the initial driver gas and driven gas pressures respectively. This equation relates the diaphragm pressure ratio to the incident shock Mach number. The driven gas pressure is generally chosen first, and the driving gas pressure is then calculated by using Eq. 13.

4.4 SELECTION OF TUBE LENGTHS AND CROSS-SECTIONS

The next step involves the selection of the suitable tube lengths, tube cross-sections and tube material. The driven section is usually about four to six times as long

as the driving section. The design run time establishes the length of the driver and driven sections. Shorter lengths reduce the design run time substantially. Longer than necessary driven section lengths may increase the run time a little, but the incident shock wave may be attenuated considerably thereby reducing the stagnation properties. Moreover, long driven sections lead to the development of the boundary layer behind the traveling shock and eventually turbulent pipe flow. This premature onset of turbulent pipe flow behind the incident shock wave, will effect the performance of non-reflected shock tunnels. The boundary layer leads to shock bifurcation and thus effects the uniformity of the gas properties behind the reflected shock wave.

In the case of straight-through or incident shock tunnels, the driver section length χ_4,for a specified run time, is calculated by using Eq. 1. The minimum length of the corresponding driven section,χ_1, is calculated by

$$\chi_{1\min} = \left[\frac{\tau_c + \frac{\chi_c}{W_R}}{1/W_S + 1/W_R} \right] \tag{14}$$

where χ_c is the distance between the point of intersection of the reflected rarefaction head and the contact surface, and the diaphragm station.

Shock tunnels can either be circular or rectangular in cross-section. Rectangular cross-sections facilitate convenient mounting of sensors and transducers along the tunnel wall. Spectroscopic studies and optical flow studies can be easily carried out in the

shock tube by installing glass windows along the tube. Such installation is very difficult in the case of tunnels with circular cross-sections. However, if the main interest is to analyze the flow in the tunnel nozzle, then the cross-section becomes insignificant. Rectangular cross-sections are quite prevalent in the case of low pressure shock tubes, or those used for spectroscopic studies. Circular cross-sections are common in shock tubes and tunnels working at high pressures. Circular cross-section offers a higher structural rigidity than rectangular cross-section and tubes with circular cross-sections are very easy to join.

The most commonly used materials for high pressure shock tube/tunnel construction are extra strength steel (schedule # 80), double extra strength steel (schedule # 120), or stainless steel (used in tunnels operating with corrosive gases). Shock tubes working at low pressure, especially those for chemical kinetics research can be made of Pyrex glass.

4.5 NOZZLE DESIGN

Finally, an appropriate nozzle has to be designed. This nozzle can either be a half nozzle or a full nozzle. A half nozzle usually has a flat bottom piece and a contoured top piece, while in a full nozzle both the halves are contoured pieces. This nozzle contour is usually designed by the method of characteristics, which produces a surface that ensures shock free expansion of the fluid within the nozzle. However, in some cases this contour can be a "straight" machined surface. In either case the nozzle

has a fixed exit to inlet area ratio to ensure isentropic, supersonic expansion to the design Mach number. Hence the contour has to produce the appropriate areas of cross section along the length of the nozzle.

The nozzle can be a converging-diverging nozzle, or a diverging nozzle. A converging-diverging nozzle accelerates subsonic flow to supersonic or hypersonic speeds. A diverging nozzle on the other hand accelerates the already supersonic flow to a higher Mach number. So the converging-diverging nozzle, as the name indicates, converges from the inlet cross-section to a relatively small throat, and then diverges to the exit cross-section. A diverging nozzle starts out from the throat and diverges to a larger cross-section. The absolute areas and the corresponding area ratios at different locations along the axis of the nozzle, depend only upon the flow Mach numbers. This, however, is not the case for subsonic flows where the Mach number at every cross-section depends upon both the area ratios and the corresponding pressure ratio (ratio of the local stagnation pressure in flow to the local static pressure at the cross-section in consideration). In some cases a transition nozzle can be employed. A transition nozzle has a short constant area duct that forms the throat of the nozzle, while the rest of it is just diverges. Nozzles are usually made of either steel or aluminum. More details on the design, starting mechanism, and general isentropic flow relations for nozzles can be found in any classic compressible fluid flow text.

CHAPTER 5

DESIGN OF THE TEST FACILITY

The overall sketch of the shock tunnel is given in Fig. 5. The shock tunnel was designed based upon the major design attributes and equations discussed in chapter 4.

5.1 RUN TIME AND TUBE LENGTHS

In order to effectively test the skin friction balances in the tunnel, a run time of at least one millisecond is required. However, since shock tunnels have fairly complicated flows associated with them it was desirable for the tunnel run time to be in excess of one millisecond. The driven tube length was chosen to be 20 feet (6.096 ms). This was because it was the longest single piece pipe available and anything longer than this would only result in unwanted shock attenuation. Once the driven section length was chosen, the driving section length was chosen to be 8 feet (2.4384 ms). This was done to ensure that the corresponding length ratio was within the design limits. For these tube lengths and the regular driver gas pressure of 200 psig (1.378 MPa gage) the air driver yielded a run time of about 7 msec while the helium driver yielded 4 msec of run time.

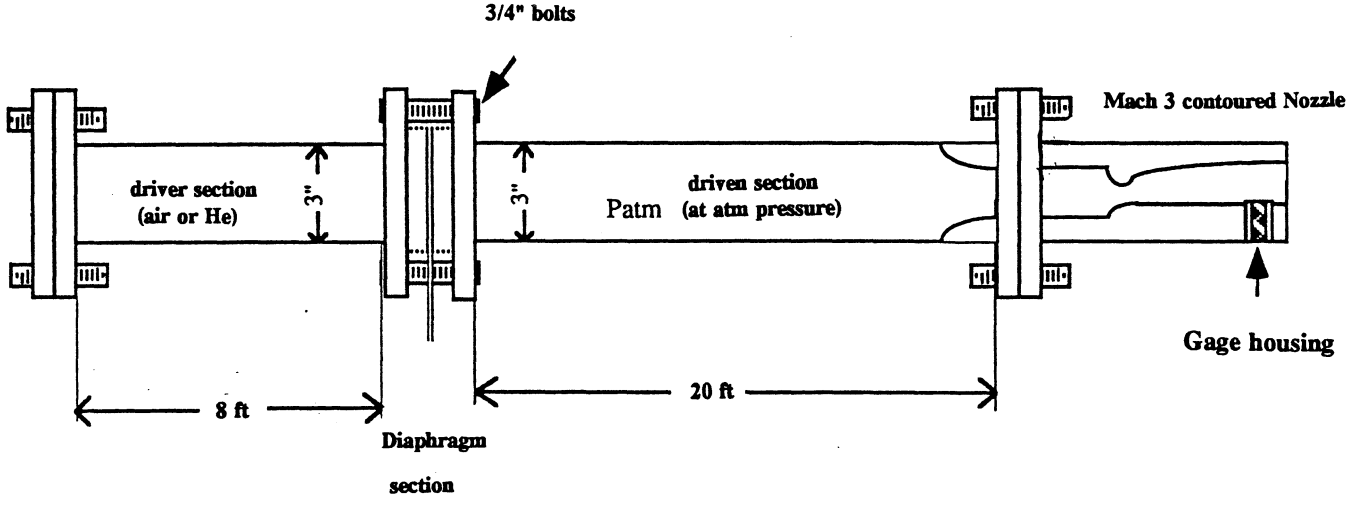

Figure 5 : The Shock Tunnel

These run times were calculated using Eq. 3 . Thus, the chosen tube lengths resulted in a run time greater than the desired minimum run time of 2 msec.

5.2 TEST GASES AND TEST PRESSURES

Initially air was chosen both for the driving and driven gases. This is because the driven section was left open to the atmosphere and it was decided that a like gas be used for the driving gas. Also, for the same diaphragm pressure ratio, and driven section length, a heavier gas with a larger specific heat ratio gives a longer run time. After testing the tunnel with an air driver, helium was used as the driving gas. This is because helium, being a lighter gas with a larger specific heat ratio, produced much higher total temperature and pressure.

The initial driving gas pressure was chosen to be 200 psig (1.378 MPa gage) to match tests that were previously conducted in a Ludwig tunnel. The Ludwig tunnel produced supersonic flow for about 40 milliseconds. To avoid the complications of evacuating the driven section ambient pressure was chosen to be the driven gas pressure.

5.3 TUBE MATERIAL AND CROSS-SECTION

Both the driver and driven sections were made of high strength carbon steel. The cross-sections were circular. This is in accordance to the design feature that circular cross-sections offer the highest structural rigidity. Also, tubes with circular cross-sections are easy to attach. Both the pipes have been fitted with 600 psi (4.137 MPa),

forged steel , slip -on-flanges, which have been welded onto the pipes.

5.4 DIAPHRAGM HOLDER

Mylar was chosen for the diaphragm material. Mylar has good and repeatable burst characteristics. Moreover, it is very cheap and thus economical to use. A diaphragm holder which just mounts onto the outer lips of the flanges of the driving and driven sections, was designed to house the Mylar diaphragm. The purpose of this holder was to prevent the diaphragm from being stressed or flexed during the mounting process. Pre-stressing of the diaphragm results in non uniform stress concentrations in the diaphragm material, resulting in poor diaphragm rupture characteristics. A sketch of the diaphragm holder is given in Fig 6. The diaphragm, which is 0.01 in.(0.254 mm) thick, usually bursts at a pressure of about 200 psig (1.378 MPa gage). However, it has been observed that a controlled and gradual pressurization of the driving section not only results in a marginally higher burst pressure but also petals out the diaphragm better. The diaphragm holder has O-rigs both on the outside and on the inside. The O-rings on the outside achieve leak proof seal between the outer lips of the pipe flanges and the diaphragm holder, while their inner counter parts prevent leakage from the gap between the Mylar diaphragm and the frame.

5.5 FLOW MACH NUMBER AND ASSOCIATED NOZZLE

A flow Mach number of 3 was chosen. To facilitate the easy installation of the

skin friction and heat flux transducers it was decided that the nozzle have a flat bottom piece. A Mach 3 2-D nozzle designed by Dr.R.Bowersox of the department of Aerospace and Ocean engineering of Virginia Tech, was attached to the end of the driven section. Figure 6 gives the sketch of this nozzle. This contoured nozzle was designed using the method of characteristics. Both the top and bottom pieces were made of a two inch wide aluminum block. The inlet and exit areas of cross-section are four square inches each. The throat of the nozzle has a cross-section of one square inch, two inches wide and one quarter inch deep. The throat cross-section was so chosen that the incident shock wave would be almost completely reflected back into the driven section, thus producing a region of almost stagnant gas. Once the throat was chosen, the inlet and exit areas were selected to produce Mach 3 flow at the nozzle's exit. In front of the nozzle is a settling chamber, which is a three inch long rectangular duct. This chamber allows for the stabilization of the weak subsonic flow at the nozzle entrance and further facilitates the insertion of transducers to measure the flow conditions behind the reflected shock. The settling chamber is followed by a converging section that leads to the throat of the nozzle. After the throat the bottom half of the nozzle is a flat piece while the top piece of the nozzle is contoured to produce shock free supersonic expansion. The nozzle has side windows which facilitate Schlieren photography, thus making it possible to analyze the flow visually. One of the most important features of Schlieren or shadowgraph photography is the direct visualization of the boundary layer, free stream turbulence (evident from the eddies), shock waves and other contact discontinuities. The

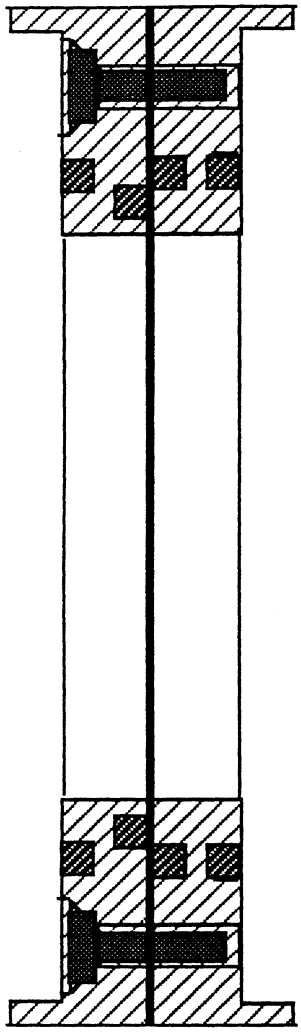

4 O-rings
4 screws
2 pins

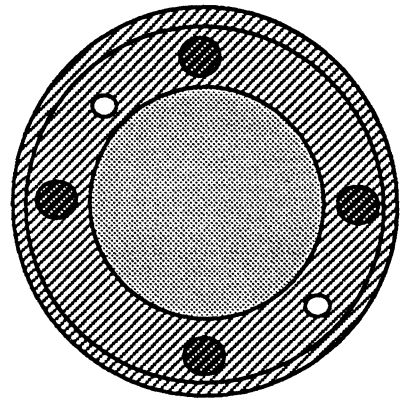

Figure 6 : Diaphragm Holder

windows have been attached to the nozzle blocks by using allen screws. A schedule # 80 blind flange was used to hold the nozzle. This blind flange had a square hole, 2 inches by 2 inches, cut in it to match the inlet of the nozzle. Holes were drilled and tapped into this blind flange and nozzle block to facilitate the attachment of the nozzle to the blind flange by using counter-sunk allen screws. This flange nozzle assembly was then bolted onto the pipe flange of the driven section.

5.6 SUPERSONIC DIFFUSER

A supersonic diffuser with a ramp angle of 10 degrees was designed and attached to the nozzle. The primary intention behind this installation was to prevent the occurrence of adverse pressure gradients and thus prevent separation of the boundary layer at the nozzle's exit. The ramp angle was so chosen that the ratio of the flow Mach numbers satisfied the condition $[(M_2 / M_1)]^2 \geq 0.55$, where M_2 and M_1 are the flow Mach numbers downstream and upstream of the oblique shock wave formed at the nozzle-diffuser junction, respectively. This condition was experimentally established by Dr. J.A. Schetz of the department of Aerospace and Ocean Engineering of Virginia Tech.

5.7 TUNNEL AND NOZZLE SUPPORTS

The driving and driven sections were supported by wall brackets that were bolted into the wall. In order to enhance it's rigidity and thus minimize the recoil, the nozzle

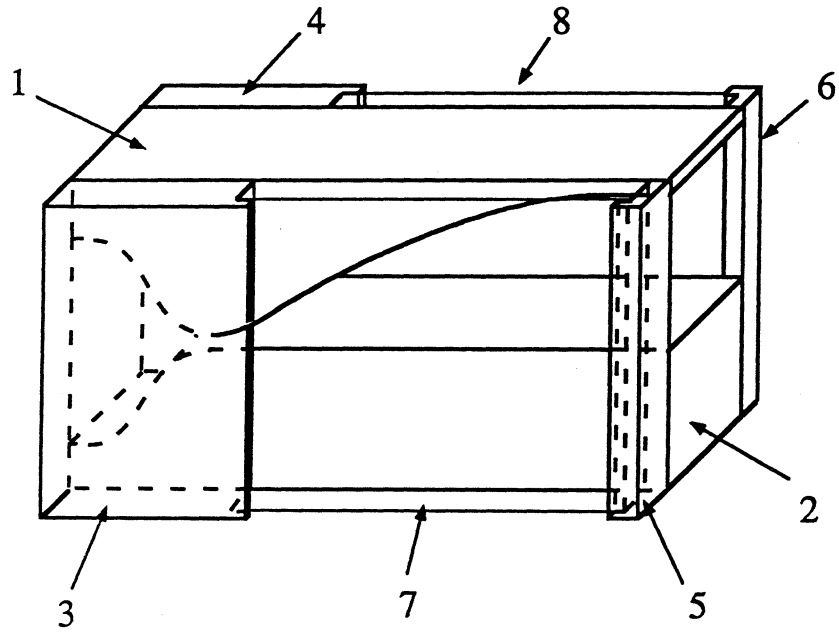

Parts 1&2: Nozzle contour blocks
Parts 3-6: Aluminum side blocks
Parts 7&8: Plexiglass windows

Figure 7 : Mach 3 Nozzle

was supported by an end plate that bolts into the wall. Figure 8 gives a sketch of the end plate and Fig. 9 which shows how the end plate is attached to the pipe flange of the driven section.

5.8 GAS SUPPLY LINE

The driving section was fed from a gas tank via the gas supply line. This supply line was made up of pipe connectors and swage lock fittings. It had a pressure gage installed to check the pressure of the driving gas. A one way check valve was also installed to prevent the back flow of the driving gas into the cylinder. Also, a pin valve was included in this gas supply line. This valve served as a pressure relief valve. Figure 10 shows this supply line.

5.9 SHOCK TUNNEL INSTRUMENTATION

Strain gage pressure transducers were used to measure the total and static pressures in the nozzle. These pressure transducers have an active four-arm wheatstone bridge and when pressurized develop a bridge unbalance which is recorded as a voltage output. Kulite and Lucas Schaevitz pressure transducers were used for measuring pressure in all the test runs and are described in detail in Appendix A. Strain gage signal conditioners and voltage amplifiers were used for boosting the output signal from these transducers. The operational features of these amplifiers are discussed in Appendix A. Thermocouples were specially made to record the total temperature in the settling

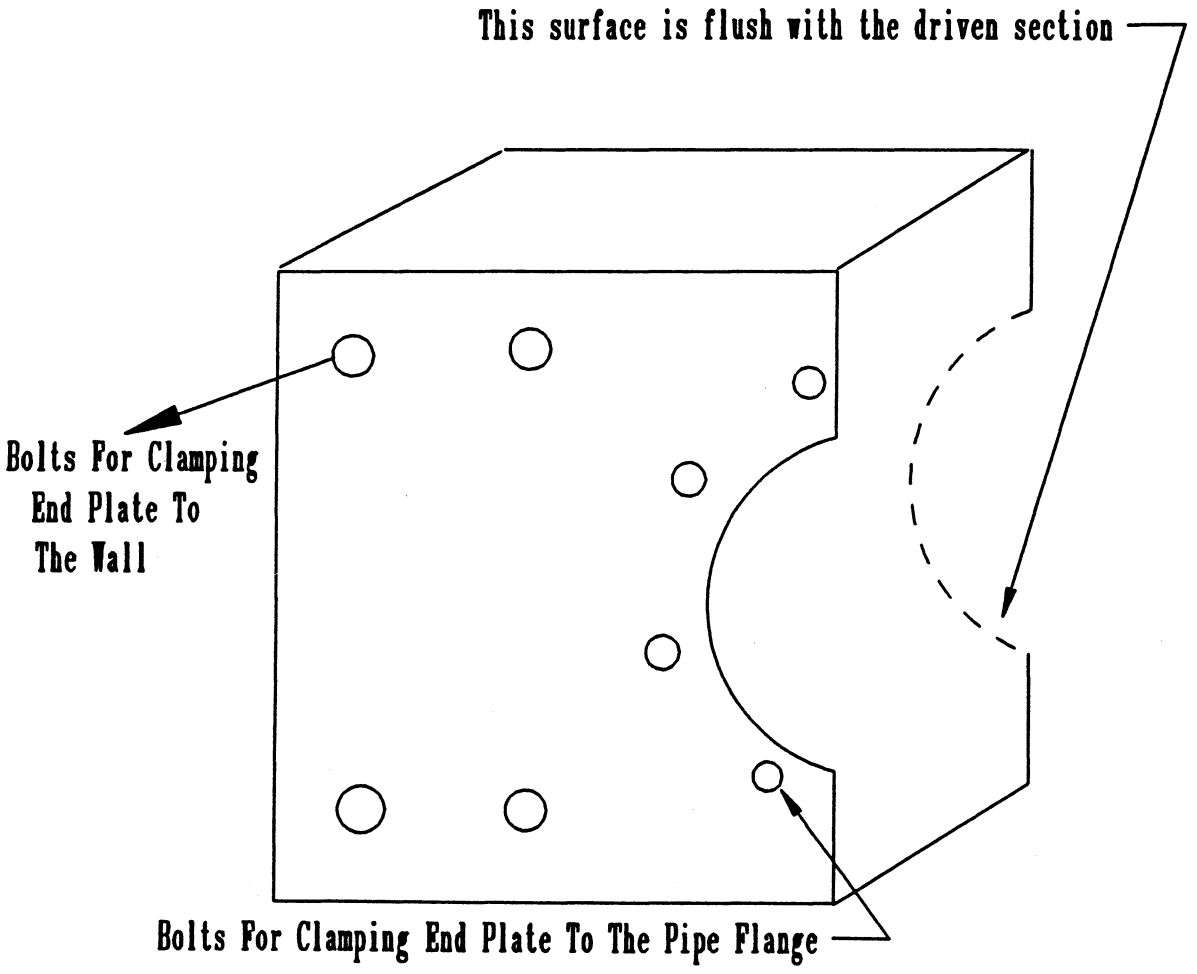

Figure 8 : End Plate Attachment for the Nozzle

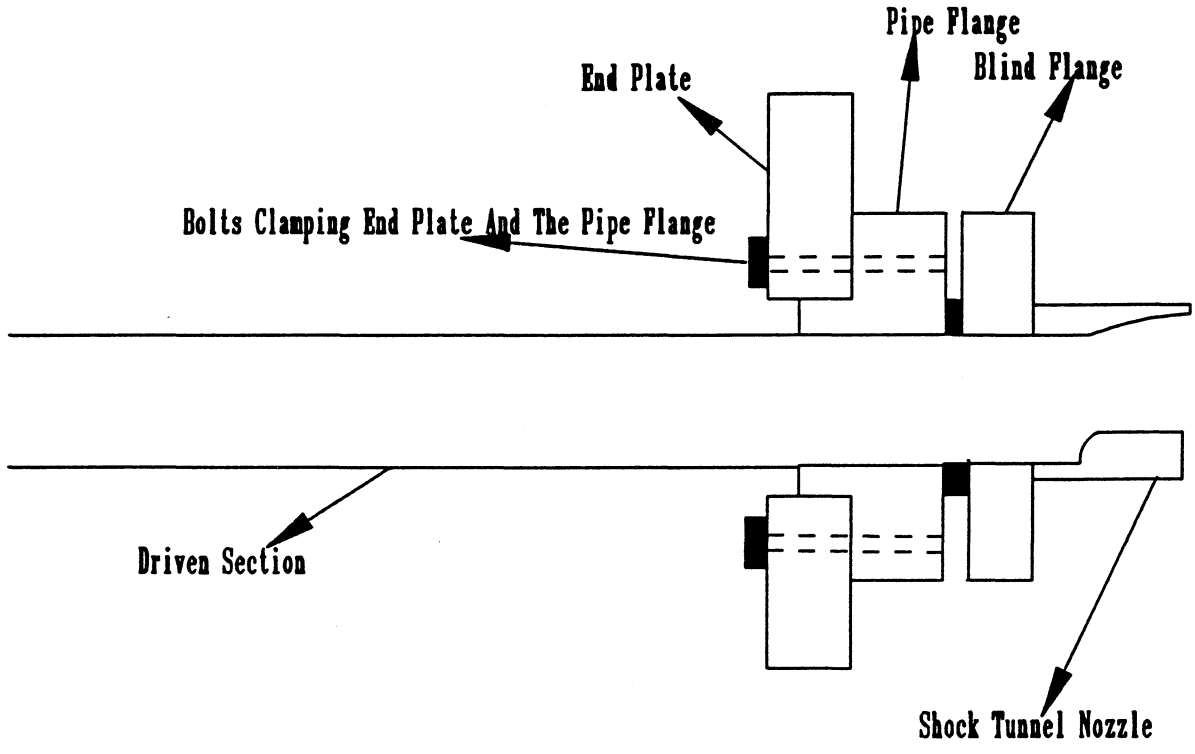

Figure 9 : Shock Tunnel With the End Plate

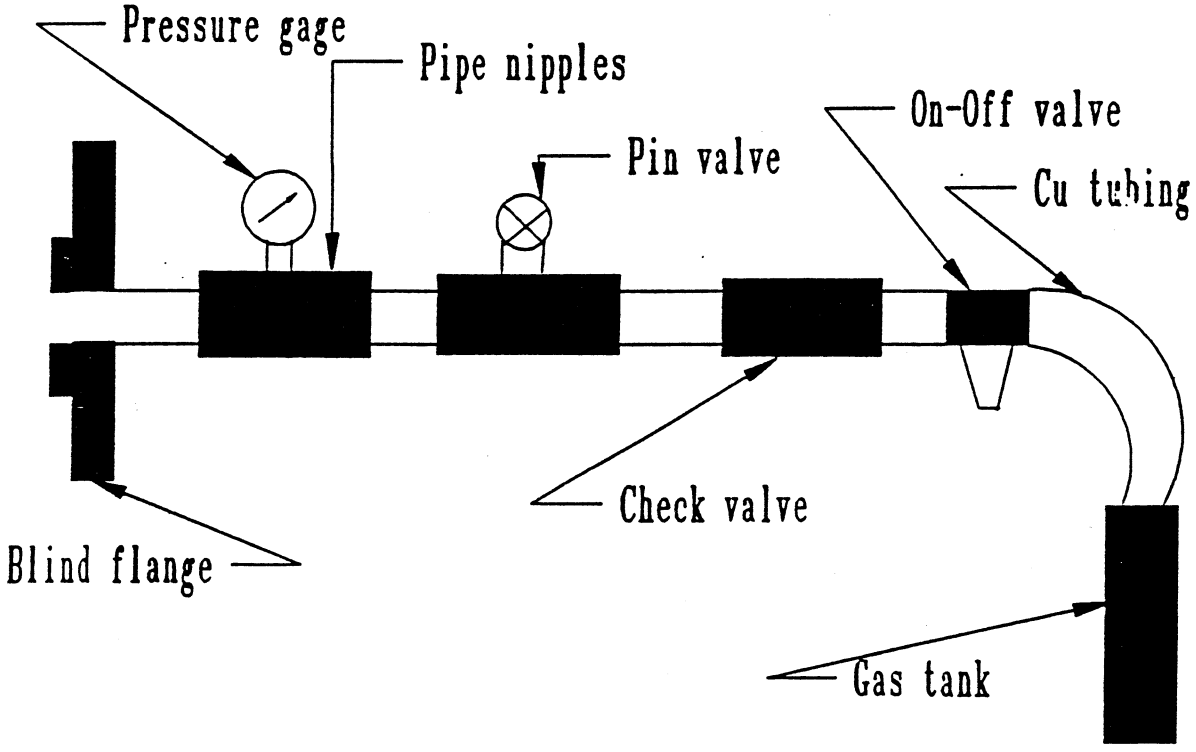

Figure 10 : Gas Supply Line

chamber of the nozzle. Because of the very short run times the thermocouples had to have low time constants to capture the transient temperature. Hence, the corresponding bead size had to be extremely small, with a typical diameter being 0.003 inches (0.0752 mm). Consequently, the fabrication of these thermocouples and the interpretation of the corresponding temperature measurements was challenging. First-order transient temperature estimation techniques were used to obtain an estimate of the maximum total temperature of the fluid. The rest of this section focuses on the design and fabrication of these thermocouples and the implementation of the first-order temperature estimation techniques.

5.9.1 TEMPERATURE SENSORS

The thermocouple wires used were one thousandths of an inch in diameter, with the corresponding bead size being 3 times the wire diameter. They were welded together using a thermocouple welder. To facilitate ease in construction and handling of the thermocouples, these 0.001 inch (0.0254 mm) diameter wires were then soldered on to their 0.003 inch (0.0762 mm) diameter counterparts. A ceramic tube with two cylindrical holes in it was chosen for the probe housing. The thermocouple wires were inserted in it, one in each, and pulled down just so that the bead barely stuck above the ceramic head. The ceramic piece was epoxied in a hollow metal bolt, and this bolt was then inserted into the side plate of the settling chamber of the nozzle. To maintain a constant reference temperature, a 0.003 inch (0.0762 mm) alumel wire was soldered

onto the corresponding chromel wire of the thermocouple and this junction was immersed in an ice bath. The sketch of the thermocouple and its housing is given in Fig. 11. The thermocouple produces a thermoelectric voltage which is directly proportional to the temperature difference between the bead and the cold junction. For the type K thermocouple used the sensitivity varies from 40 μV/°C at 20°C to 43 μV/°C at 650°C. Because the measured thermocouple temperatures were between 20°C and 200°C a constant sensitivity of 40 μV/°C was used.

5.9.2 FIRST ORDER TRANSIENT TEMPERATURE FIT TECHNIQUES

Owing to the slow response time of the thermocouples relative to the flow the analytical techniques had to be used to estimate the total temperature of the fluid from the measured thermocouple data. Two different first-order transient temperature estimation techniques were used for this purpose. In both the techniques the thermocouple response was modeled as a step change in temperature. The implementation of these techniques required the knowledge of the time constant of the thermocouples. One time constant of a thermocouple is defined as the time it takes for the difference in temperatures of the thermocouple bead and the surrounding environment to reduce to 63.2% of the initial difference. The following is a description of the procedure used for calculating the theoretical time constant of the thermocouples followed by a discussion of the two temperature estimation techniques.

To analyze the transient temperature of the thermocouple bead it was assumed that

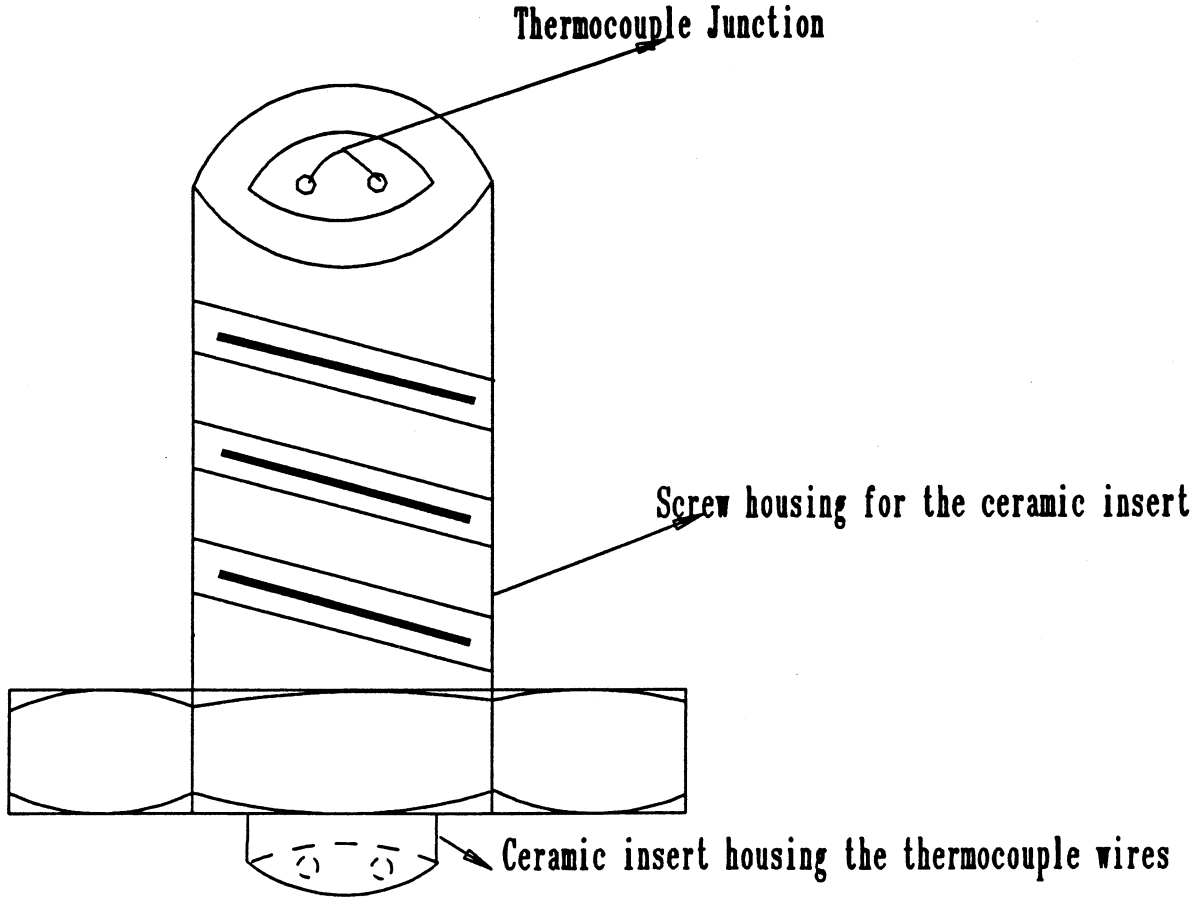

Figure 11 : Thermocouple And its Housing

the heat transfer to the bead was primarily due to convection from the fluid in the settling chamber. The effects due to radiation and the internal temperature gradients in the bead were neglected. The basic heat transfer equation is

$$mc_p\frac{dT}{dt}=hA_{sur}(T_\infty-T) \tag{15}$$

where m is the mass of the thermocouple bead, c_p is its specific heat coefficient, h is the average convective heat transfer coefficient, A_{sur} is the surface area, T_∞ is the local free-stream temperature of the fluid (which for the low speed flow in the settling chamber is close to the total temperature), and T_i is the initial temperature of the bead. The solution to the first order differential equation in Eq. 15 is

$$T=T_\infty-(T_\infty-T_i)e^{-\frac{t}{\tau}} \tag{16}$$

where the time constant τ of the thermocouple is $\tau = mc_p/hA_{sur}$.

In both the air and helium runs the test gas is always air in the settling chamber. The average Nusselt number was calculated using the equation due to Incropera (1985)

$$Nu_{D_{avg}}=2+\left(0.4Re_D^{0.5}+0.06Re_D^{2/3}\right)Pr^{0.4}\left[\frac{\mu_\infty}{\mu_s}\right]^{1/4} \tag{17}$$

where $Nu_{D(avg)}$ is the average Nusselt number based on the diameter of the thermocouple junction, Re_D is the local Reynolds number, Pr is the Prandtl number of the fluid, μ_s is the absolute viscosity of the fluid at the surface and μ_∞ is the absolute viscosity of the

fluid in the free-stream. The Reynolds number $Re_D = \rho VD/\mu$ in the plenum is based upon the local velocity V=0.14 a, where 0.14 is the local flow Mach number and a is the local sound speed. To evaluate the fluid properties in Eq. 17 the average film temperature was calculated assuming that T_∞=618 K (the theoretically predicted total temperature of the fluid) and T_i=293 K. The local convective heat transfer coefficient is obtained from the Nusselt number as $h = \{Nu_{Davg} K/D\}$. The calculated value for h was 4362.93 W/m^2 K, and the corresponding time constant τ was 10 msec. Even though this time is very small, it is still large relative to the flow time. Therefore transient temperature curve fit techniques were necessary to estimate the maximum temperature of the stagnant fluid.

Technique 1: To get a straight line fit between T and t, Equation 16 can be rewritten as

$$\ln\left[\frac{T_\infty - T}{T_\infty - T_i}\right] = -\frac{t}{\tau} \qquad (18)$$

Then a linear regression can be performed on the variables $\ln[(T_\infty - T)/(T_\infty - T_i)]$ and t and the corresponding output is

$$\ln\left[\frac{T_\infty - T}{T_\infty - T_i}\right] = -\frac{t}{\tau} + \text{const} \qquad (19)$$

where const is the constant of regression. In Eq. 19 T_∞ and τ, the two unknown variables, can't be separated. Therefore, iteration was performed to get the best linear

fit for Eq. 19. The linearity of this fit is dictated by the R^2 estimate which is a statistical estimate. R^2 value of 1.0 denotes the optimum linear fit and value of 0.0 denotes the worst fit.

Technique 2: Differentiating Eq. 16 with respect to time and taking the natural logarithm of both the sides results in the expression

$$\ln\frac{dT}{dt} = -\frac{t}{\tau} + \ln\left[\frac{T_\infty - T_i}{\tau}\right] \tag{20}$$

which is the equation for a straight line with τ being the slope and $\ln[(T_\infty - T_i)/\tau]$ being the y intercept. Once the value of τ is known, it can be substituted into the y intercept term to calculate T_∞. Hence, in this technique τ and T_∞ can be separated. The slope and the y intercept for this straight line can be computed by performing a linear regression on the variables ln(dT/dt) and t.

For this technique to work it is necessary to have positive temperature derivatives. This is because natural logarithm of negative temperature gradients gives an error. Therefore in order to cut down on the noise in the measured temperature and to smooth the trace a first order 3-point formula curve fit technique was used. The corresponding formulas due to Hildebrand (1974) are

$$y_1 = \frac{1}{6}(-f_{-1} + 2f_0 + 5f_1) \tag{21}$$

where y_{-1}, y_0 and y_1 are the modified counterparts of the measured data points f_{-1}, f_0 and

$$y_{-1}=\frac{1}{6}(5f_{-1}+2f_0-f_1) \tag{22}$$

$$y_0=\frac{1}{3}(f_{-1}+f_0+f_1) \tag{23}$$

f_1 respectively. In the above equations subscript "0" denotes the center value in the 3 point cluster. Then the data points were incorporated into the Lagrange 5 point formula for calculating the temperature derivatives dT/dt. The Lagrange 5 point formula for calculating the first derivative of a function at the center point of the 5 point group is given by the expression

$$f_2'=\frac{1}{12h}(f_0-8f_1+8f_3-f_4) \tag{24}$$

For the test runs with an air driver it was estimated the temperature in the settling chamber of the nozzle starts dropping 12 msec after the arrival of the incident shock wave. Hence, only 12 msec of the measured thermocouple data was used for computations. In the case of the helium runs the reflected rarefaction head arrives in the settling chamber of the nozzle 1 msec after the incident shock wave has been detected by the thermocouple. Consequently, the total temperature starts dropping 1 msec after the arrival of the incident shock wave. So for the case of helium driver, only 1 msec of the measured temperature data was used in all the computations using technique 2. The typical sampling rate of the data acquisition system for the temperature measurements was 20kHz. So the corresponding time interval between two successive measured data

points was 0.0195 msec, the total number of data points being 2048.

CHAPTER 6

RESULTS AND DISCUSSION - FLOW MEASUREMENTS

The total pressure measurements were made through a pressure tap in the settling chamber of the nozzle. Strictly speaking this pressure is the static pressure in a weakly subsonic flow, which in this case is at a Mach number of 0.14. However, at such low Mach numbers the static pressure is essentially the stagnation pressure. Static pressure measurements were made approximately one inch from the exit of the nozzle. The corresponding area was 3.75 square inches (0.00242 m^2). The main intention in making the static pressure measurements was to confirm the starting of the nozzle and document the corresponding pressure. Total temperature measurements were made at the same location as the total pressure measurements. All the predicted flow properties were calculated by using the numerical program, which is given in appendix B.

6.1 AIR DRIVER: FLOW RESULTS AND DISCUSSION

6.1.1 TEST RUN - 200g A

The test conditions for this run were air driver at 200 psig (1.379 MPa) and 527 R (293 K) driving into air at 13.65 psig (0.0491 MPa gage) and 527 R (293 K).

The trace for the total pressure measurement is given in Fig. 12. The incident shock wave can be observed as a steep spike in the pressure trace. The pressure behind

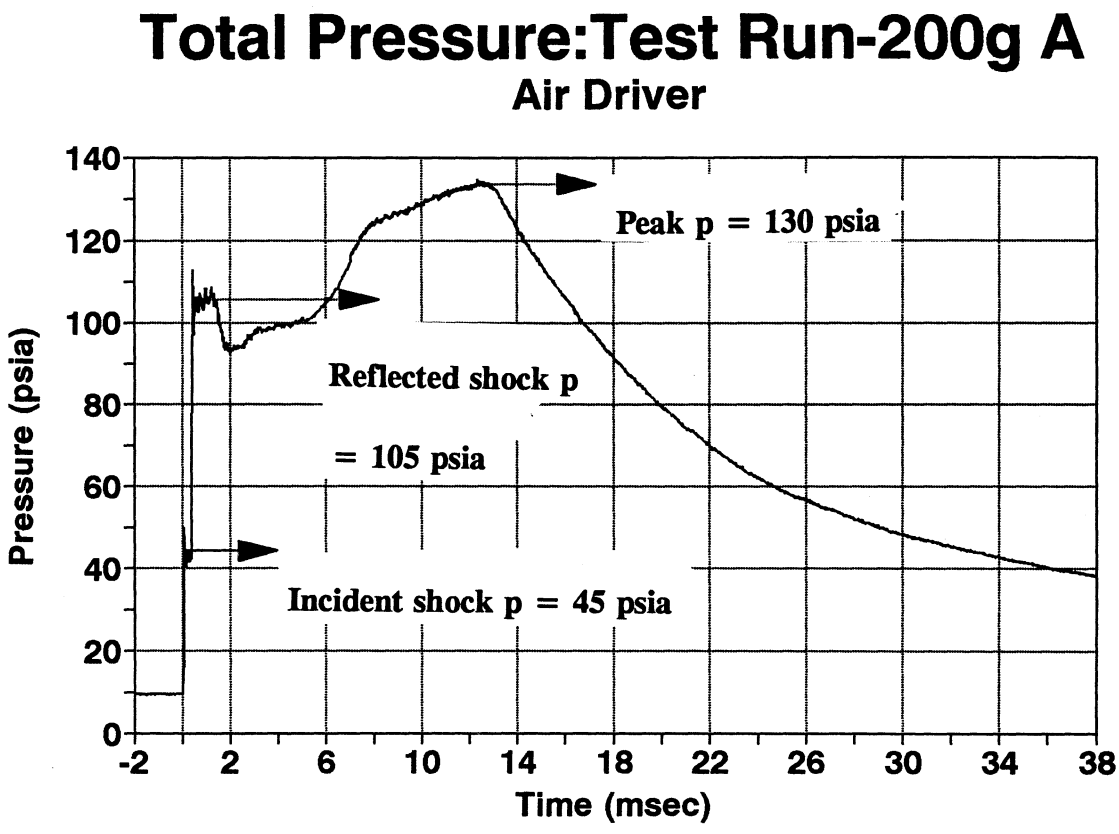

Figure 12 : Total Pressure Measurement with air driver at 200 psig and 293 K

the incident shock wave is approximately 45 psia (0.3103 MPa). The reflected shock wave is also evident as an abrupt pressure spike. The pressure behind the reflected shock wave is about 105 psia (0.724 MPa) and stays constant for about 0.5 msec. The pressure then drops and at the two msec point the pressure starts increasing. This increase in pressure continues for about 10 msec, and peaks out at a maximum value of about 130 psia (0.896 MPa). The pressure then drops. The predicted incident shock pressure for this run was 46.39 psia (0.319 MPa) which coincided well with the measured value of 45 psia (0.3103 MPa). However, the measured reflected shock pressure of 104 psia (0.7173 MPa) is considerably different from the predicted value of 129.271 psia (0.8916 MPa). Further, this pressure ascends gradually to a maximum value of 130 psia (0.8965 MPa), which is the predicted value. The reason for this anomaly is yet to be understood. Also the drop in the total pressure prior to its ascension to the peak value is yet to be understood. Although, the total pressure is not entirely constant, the conditions are steady pressure conditions.

The corresponding static pressure measurement at the exit of the nozzle is shown in Fig. 13. The incident shock wave that is transmitted through the throat of the nozzle is recorded as an abrupt pressure increase. It is interesting to note that the incident traveling shock wave attenuates a little on its transmission through the throat from 45 psia (0.3103 MPa) to 40 psia (0.275 MPa). The significance of this static pressure trace lies in its portrayal of the starting process of the nozzle. It is clear from Fig. 13 that the static pressure decreases after the passage of the incident shock wave and that it takes

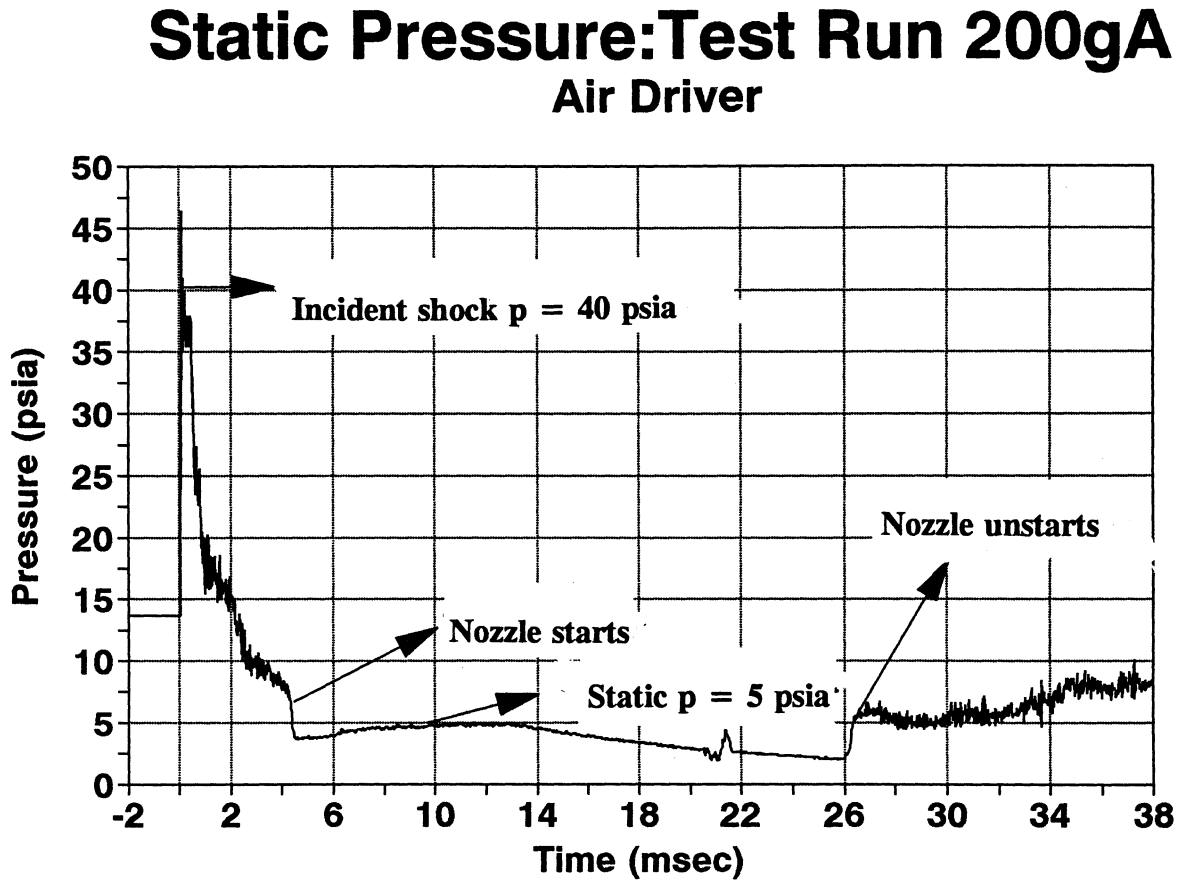

Figure 13 : Static Pressure measurement with air driver at 200 psig and 293 K

about 4 msec for it level off at a value of about 5 psia (0.0345 MPa). The abrupt drop in static pressure at the 4 msec interval, followed by an approximately constant pressure level indicates that it takes approximately 4 msec for the nozzle to start. The static pressure does, however, increase slightly (from 4 psia to 5 psia) from 4 msec to 14 msec. This matches the time during which the total pressure increases in Fig .12. Although, the ideal situation would be the one in which both the total and static pressures remain constant for the desired run time the conditions were sufficient for the required tests. The static pressure rise at 26 msec signifies the unstarting process of the nozzle.

A total temperature measurement was made in the settling chamber of the nozzle for these test conditions. Because of the low Mach number (0.14)in the settling chamber, the free stream static temperature was assumed equal to the total temperature. As evident from the temperature trace in Fig. 14 the thermocouple recorded a maximum temperature of 900 R (500 K). The predicted temperature behind the reflected shock (based upon the inviscid, adiabatic, and calorically perfect gas assumption) is 1112.4 R (618 K) behind the reflected shock for the test conditions of this test run. In order to estimate the maximum total temperature the techniques described in section 5.9.2 of chapter 5 were used. Both the techniques were successfully applied to this test run. Application of technique 1 yielded a result of 590 K for the maximum total temperature in the settling chamber. The corresponding comparison between the estimated temperature trace and the measured temperature trace is given in Fig. 15. Technique 2 estimated a total temperature of 577 K, which is close to the first estimate of 590 K

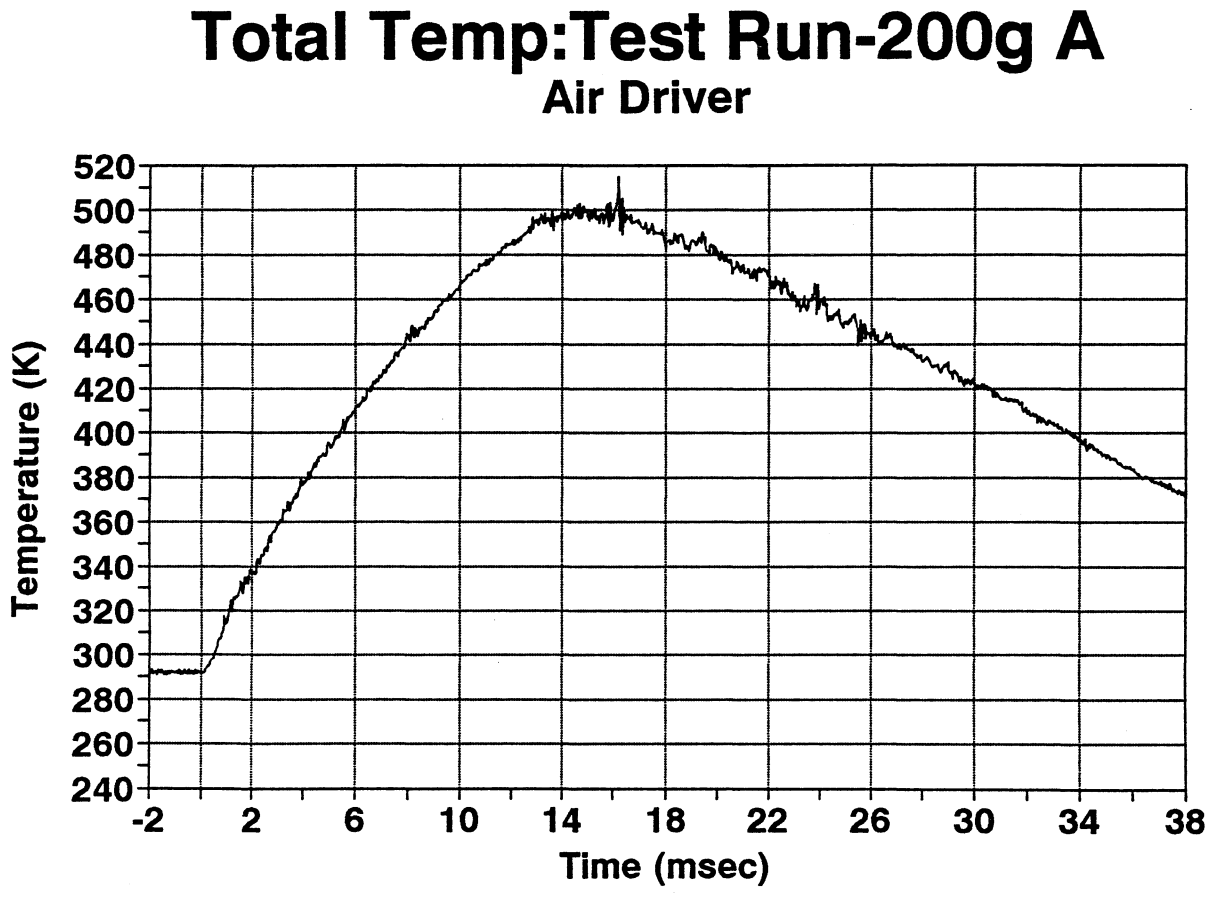

Figure 14 : Total Temperature Measurement With Air At 200 psig, 293 K

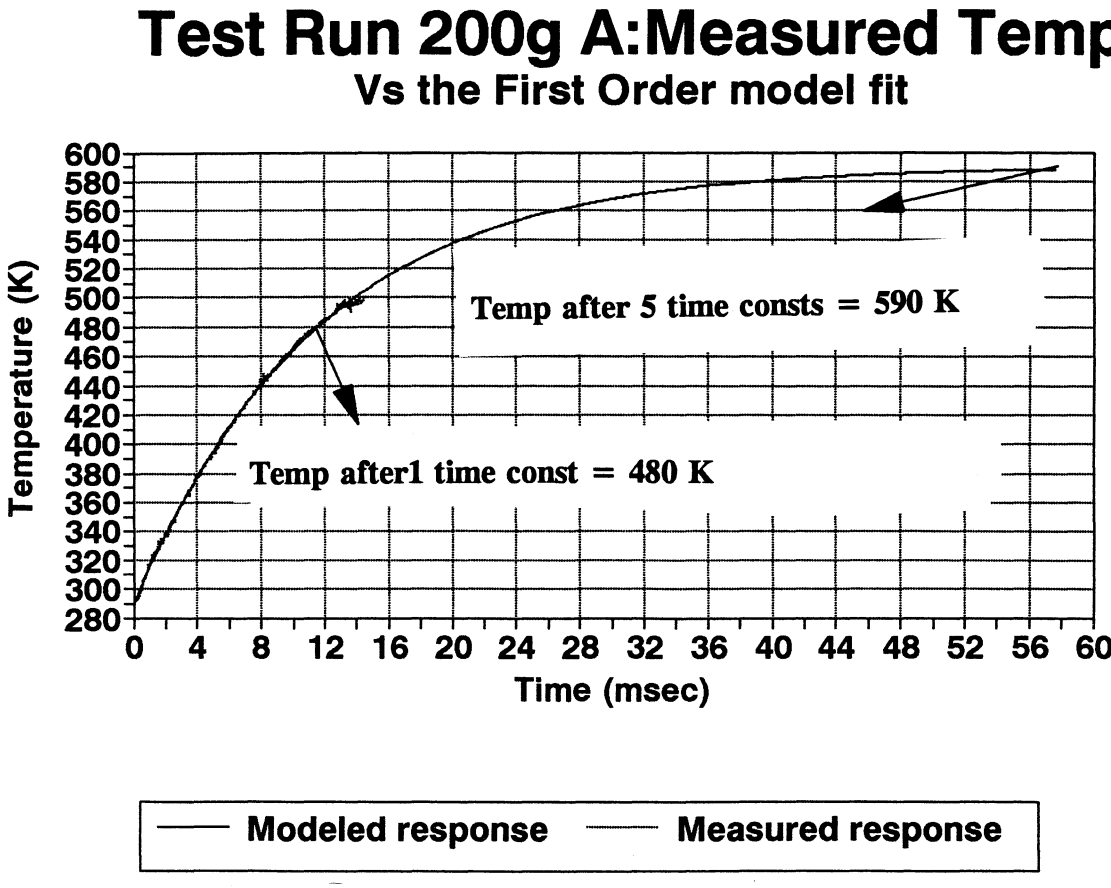

Figure 15 : Measured And Modeled Temp (Technique 1) Air At 200 psig And 293 K

validating the applicability of this technique. Figures 16 through 18 give the results of the application of this technique to the total temperature measurement of this test run.

The Mach number in a supersonic flow can be determined by knowing the local total and static pressures. The flow Mach number at the exit of the nozzle for this test run was calculated. The predicted flow Mach number is determined from the relation

$$M=\frac{A^*}{A}\left[\frac{2}{\gamma+1}\left(1+\frac{\gamma-1}{2}M^2\right)\right]^{\left(\frac{\gamma+1}{2(\gamma-1)}\right)} \qquad (25)$$

In the above expression, M is the flow Mach number, A is the local area of the nozzle, A^* is the throat area. The measured total and static pressures were inserted into Eq. 9 to obtain the measured flow Mach number. Figure 19 shows the results for the case of test run - 200g A along with the corresponding static pressure trace. The flow Mach number remained constant for the time duration for which the static pressure was approximately constant, i.e , from 4 msec to 20 msec. This gives confidence that the tunnel was operating properly over most of the run time.

6.1.2 TEST RUN - 430g A

A higher driving pressure was used to investigate if the gradual ascension in the total pressure recorded for test run - 200g A could be eliminated by the usage of a boosted driving pressure. This was conducted using an air driver at 430 psig (2.9656 MPa gage) and 527 R (293 K) driving into air at 13.65 psia (0.094 MPa) and

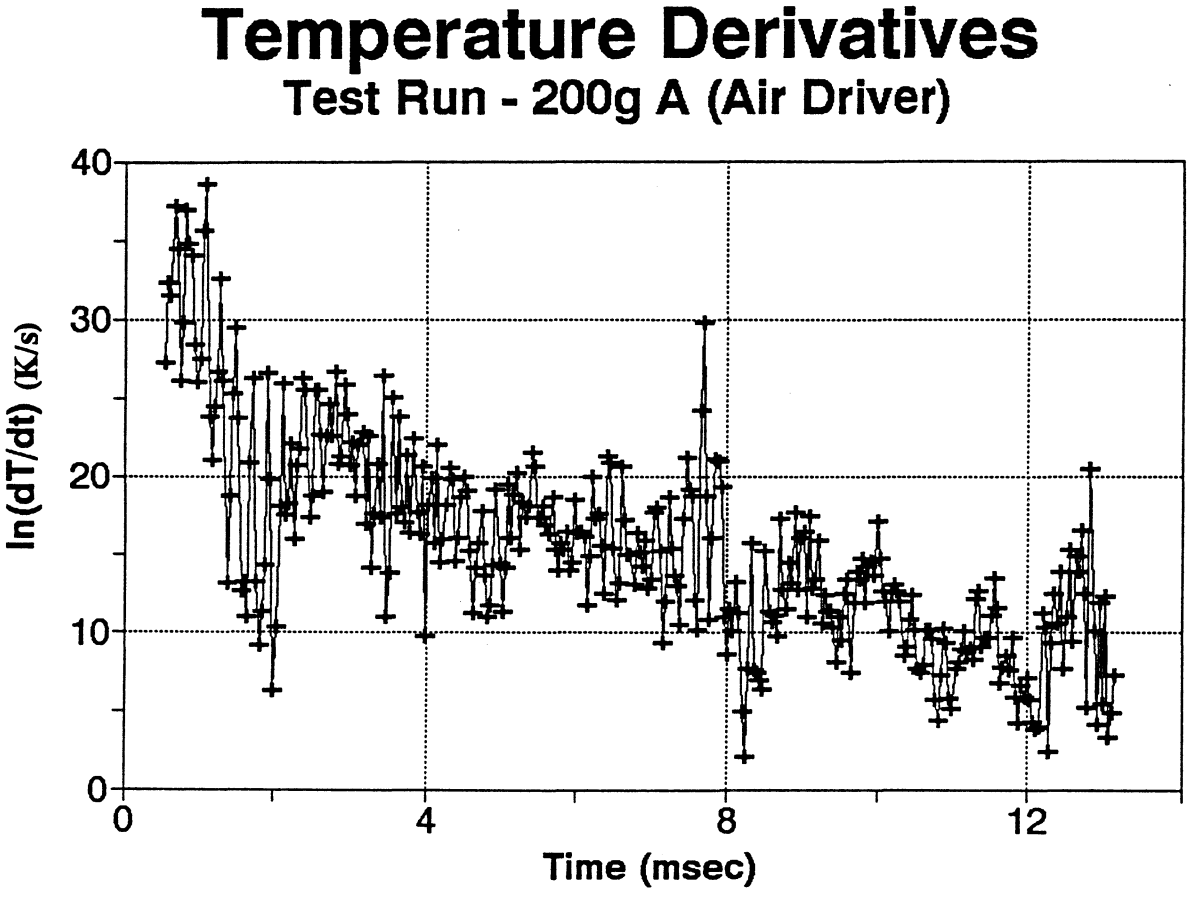

Figure 16 : Temp Derivatives With Air Dr At 200 psig And 293 K (Technique 2)

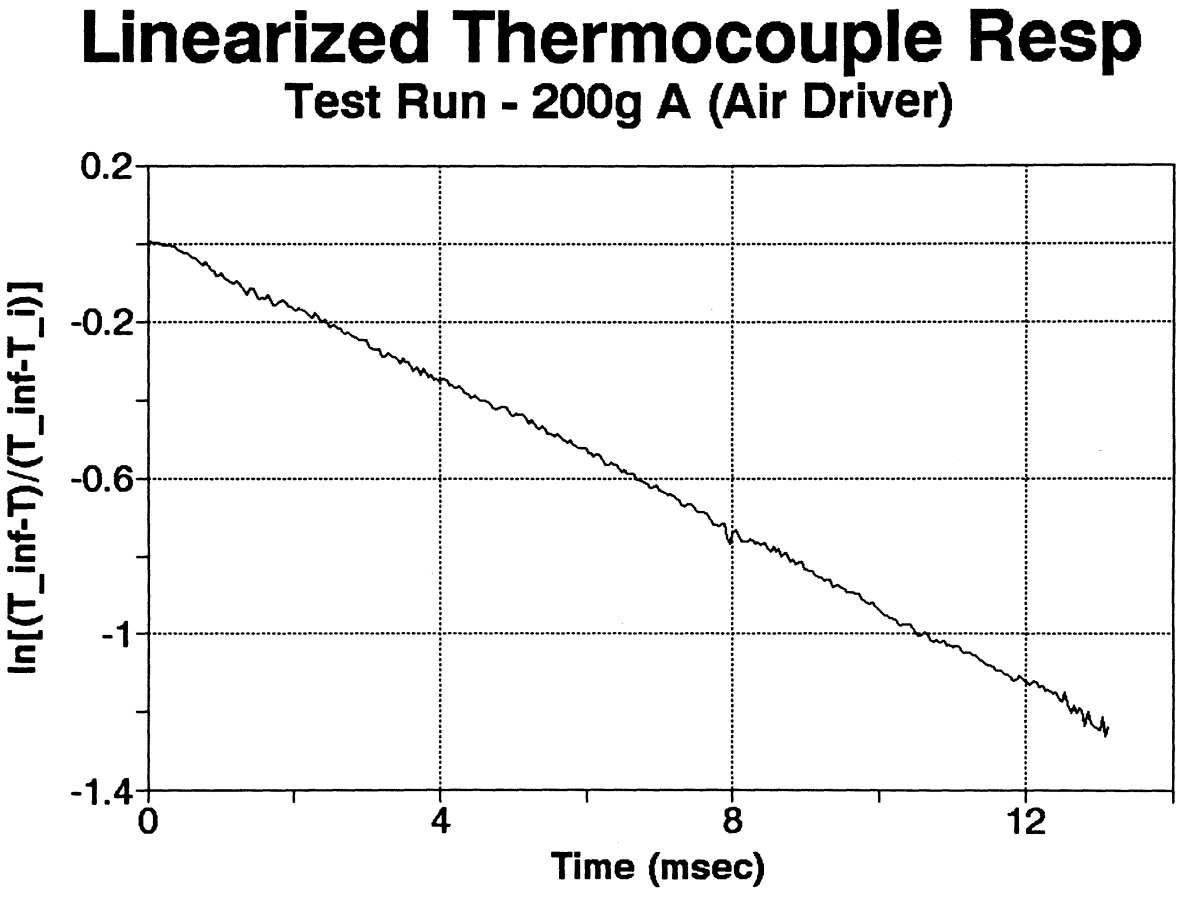

Figure 17 : Linearized Thermocouple Resp Air At 200 psig And 293 K (Technique 2)

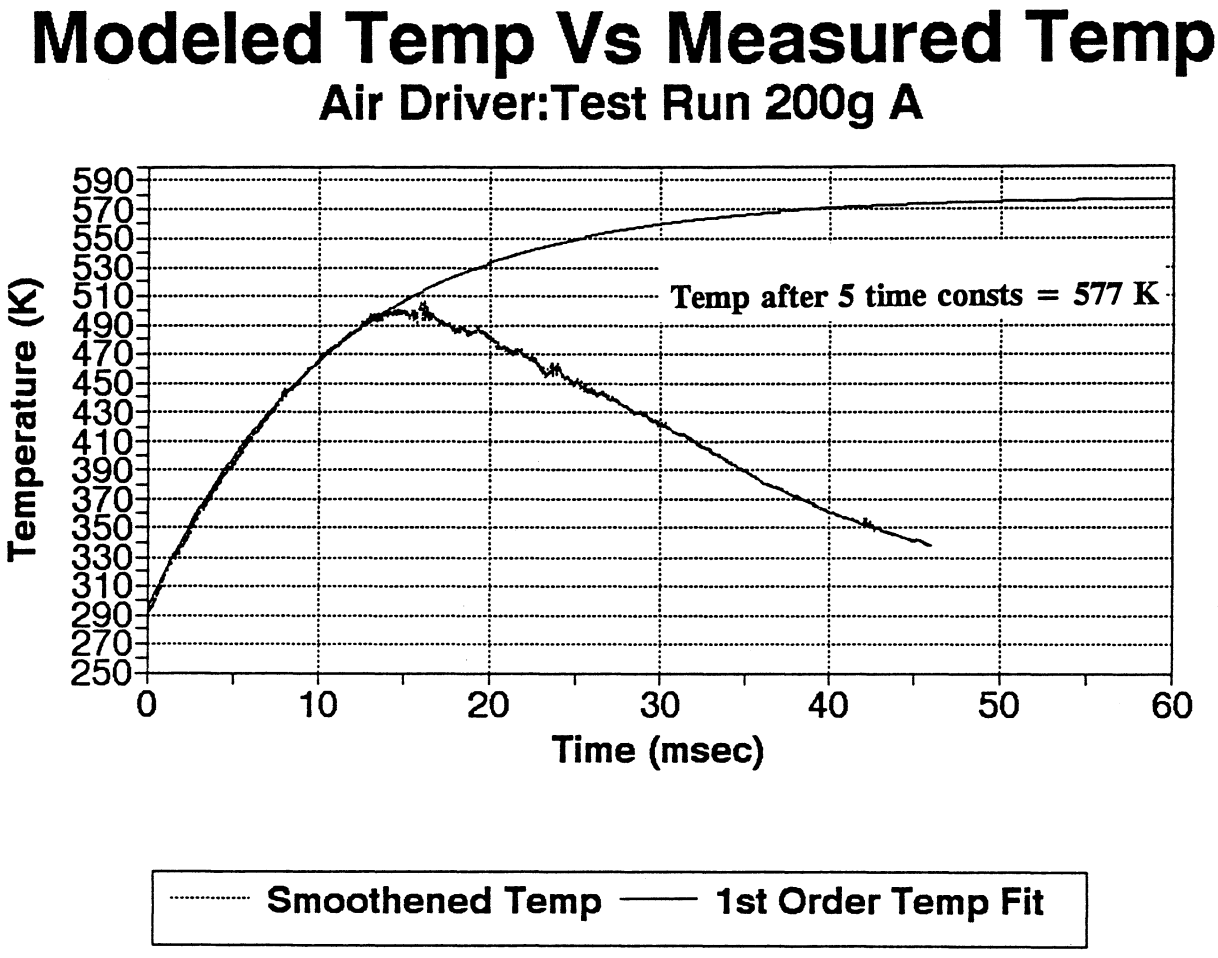

Figure 18:Measured Temp Vs Modeled Temp (Technique 2) Air At 200 psig, 293 K

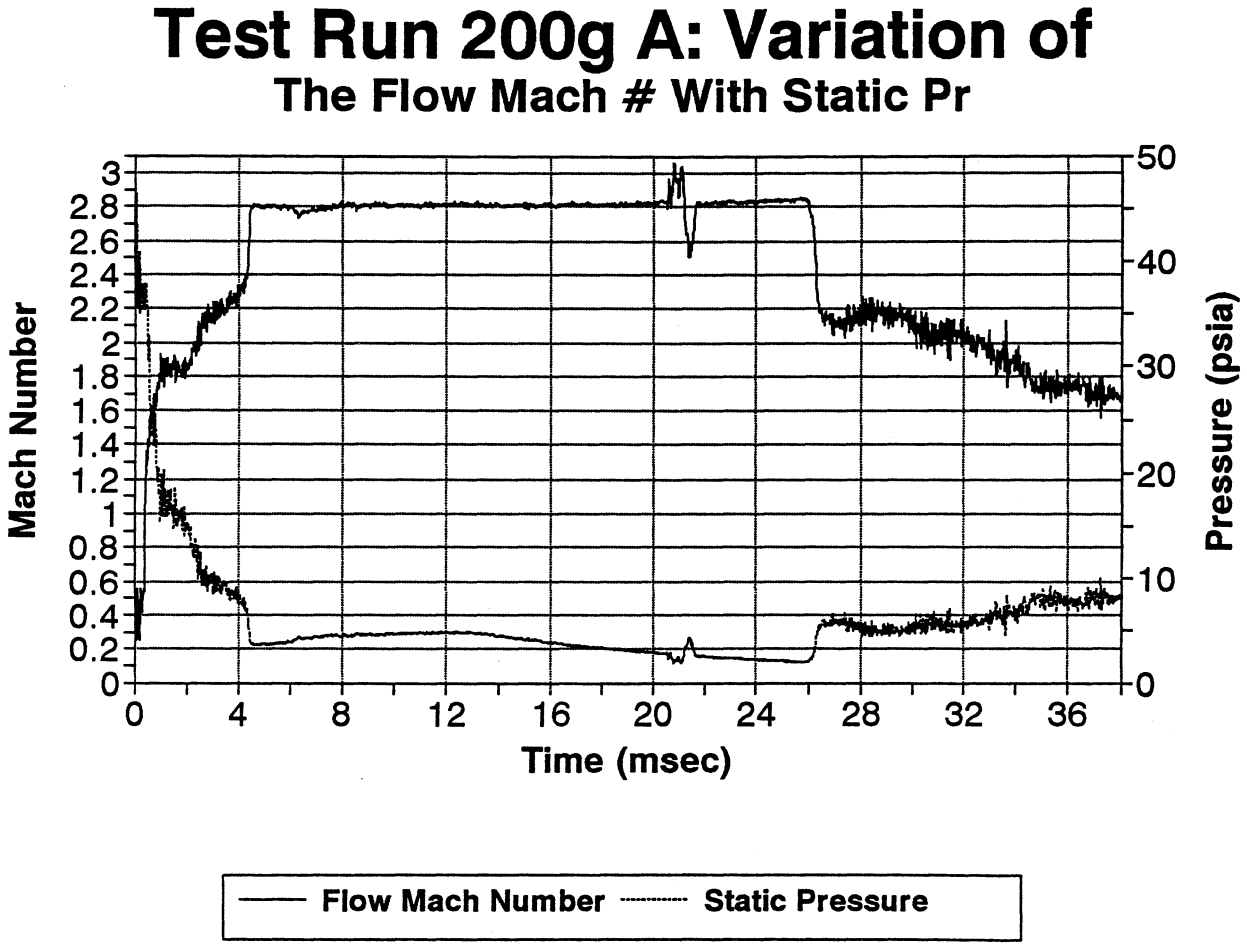

Figure 19 : Variation of Flow Mach Number With Static Pressure For Air Test Run

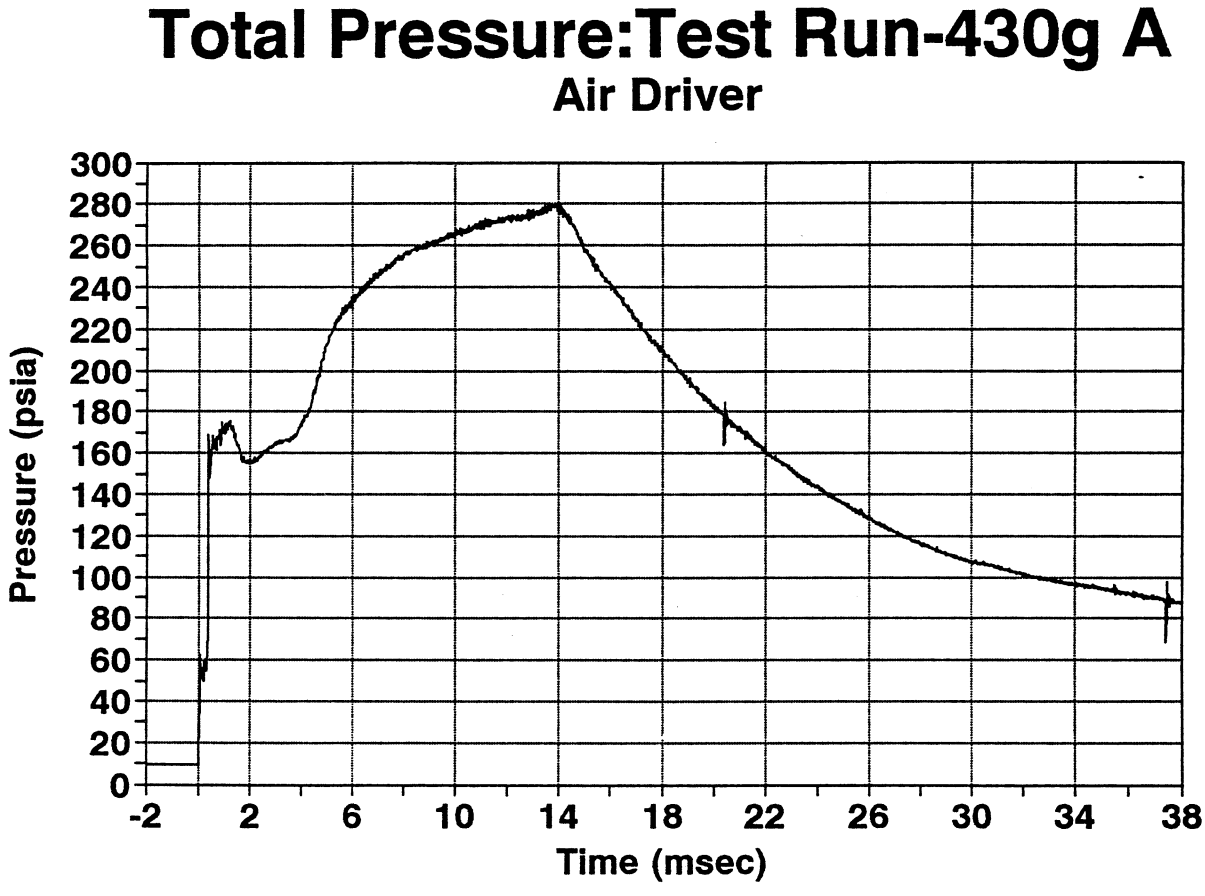

Figure 20 : Total Pressure Measurement With Air Driver At 430 psig And 293 K

527 R (293 K). Figure 20 gives the corresponding total pressure trace. From this trace it is evident that the profile of the total pressure is similar to its lower driving pressure counterpart (Fig. 12). The predicted incident shock pressure is 60.64 psia (0.4281 MPa),while the measured value is 54 psia (0.372 MPa). The predicted reflected shock pressure is 200.612 psia (1.3835 MPa) and the measured value was 165 psia (1.138 MPa). This amounts to a significant loss of 17.5% . However, the total pressure keeps increasing after the reflected shock wave and reaches a peak value of 270 psia (1.862 MPa). So the anomaly in the increase in pressure could not be understood by this test.

Because the incident shock pressures coincide reasonably well with their predicted counterparts, it was concluded that the incident shock wave is not significantly attenuated by its passage from the driven section into the settling chamber of the nozzle (involving a transition from a circular cross-section to a square cross-section accomplished by using flow transition pieces). Consequently, main issue remaining is understanding what happens next to this shock wave as it is partially reflected at the throat and partially transmitted downstream into the nozzle. Table 1 summarizes the flow conditions for the air driver tests. p_2 and p_5 are the pressures behind the incident and reflected shock waves. T_5 is the temperature behind the reflected shock wave. M_s is the incident shock Mach number and p_{static} is the static pressure at the nozzle exit.

Table 1 : Summary of Air Runs

PARAMETER	TEST RUN - 200g A		Test Run - 430g A	
	Measured	Predicted	Measured	Predicted
p_2	45.0 psia	46.39 psia	54 psia	60.64 psia
p_5	105 psia	129.271 psia	165 psia	200.612 psia
T_5	590 K (est)	618 K	*	743.279 K
p_{static}	4.246 psia	5 psia (avg)	*	6.612 psia
M_s	1.6949	1.7481	1.8798	1.9877

* Unavailable

6.2 HELIUM DRIVER: FLOW RESULTS AND DISCUSSION

Owing to a low molecular weight helium produces a stronger shock wave and hence higher stagnation conditions. This is because the shock strength p_2/p_1 is directly proportional to the driving gas to driven gas sound speed ratio a_4/a_1. So, a lighter driving gas results in a larger a_4 and thus a larger sound speed ratio. In all of the helium tests, the driving section was evacuated before filling it with helium. The results were more difficult to interpret because the non-flush mount diaphragm, Lucas Schaevitz pressure transducer was used for these measurements. The characteristics of this transducer are discussed in appendix A.

6.2.1 TEST RUN - 215g H

Figure 21 gives the total pressure trace obtained by using a helium driver at a driving pressure of 215 psig (1.483 MPa gage) and temperature of 527 R (293 K). The driven gas was air at 13.65 psia (0.0941 MPa) and 527 R (293 K). The predicted incident shock pressure for this test run was 84.547 psia (0.5831 MPa) and the measured value was 80 psia (0.552 MPa) that amounts to a shock attenuation of 4%. The predicted reflected shock pressure was 336.634 psia (2.322 MPa), while its measured counterpart was 250 psia (1.7242 MPa). This pressure stays constant for about 1.5 msec and then starts dropping. A second shock wave is recorded after 22 msec and produced an average pressure of about 120 psia (0.8276 MPa). The occurrence of this second shock wave can be explained as follows. The primary incident shock wave that is reflected at the throat of the nozzle is transmitted back into the driven section. This shock wave then travels the entire length of the tunnel until it reaches the end of the driving section, where it is re-reflected. This re-reflected shock wave once again travels the entire length of the tunnel and re-enters the nozzle producing the second recorded shock wave.

The corresponding static pressure measurement is given in Fig. 22. The incident shock wave is evident as a pressure spike. The nozzle doesn't start until a time of 2 msec, when the static pressure drops abruptly. From 2 msec to 7 msec the static pressure follows the decrease in the total pressure, dropping from about 5 psia (0.0345 MPa) to 1 psia (0.007 MPa). The static pressure increases after 7 msec until 22 msec

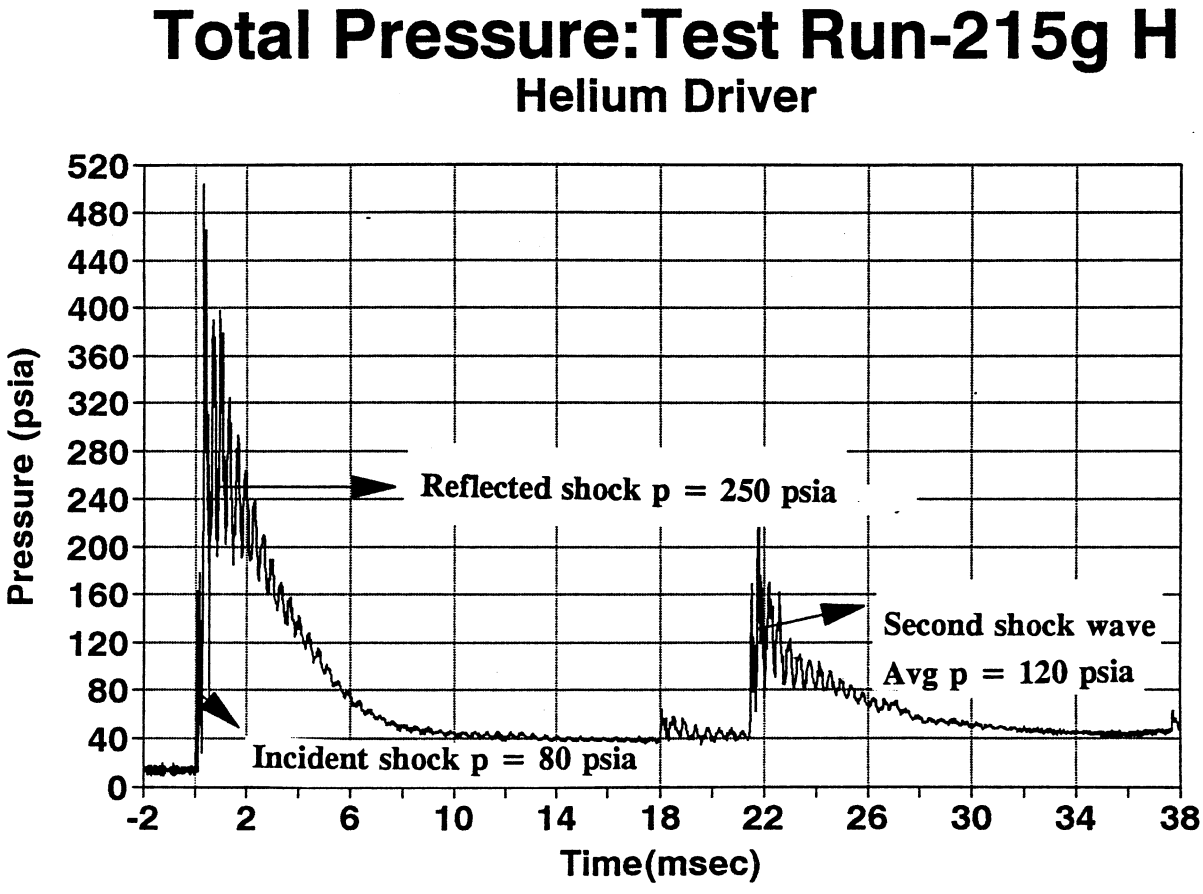

Figure 21 : Total Pressure Measurement Helium Dr At 215 psig And 293 K

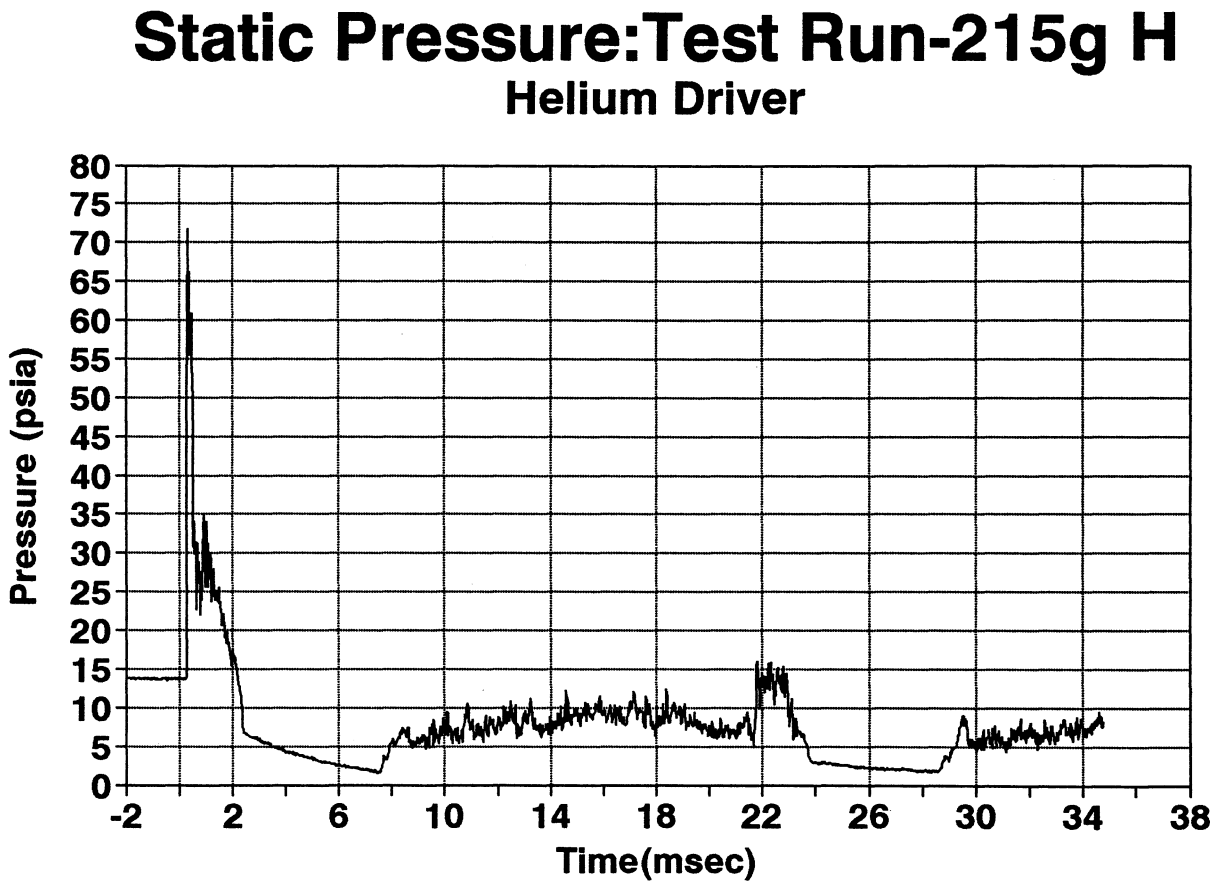

Figure 22 : Static Pressure Measurement Helium Dr At 215 psig And 293 K

when there is a sudden jump in the static pressure. This corresponds to the occurrence of the second shock wave in the total pressure trace. The remarkable feature is that this second shock wave is still capable of re-starting the nozzle, as indicated by drop in static pressure at 24 msec to 2.5 psia (0.0172 MPa).

The corresponding total temperature in the settling chamber is shown in Fig. 23. Although the response time of the thermocouple, about 10 msec, was large relative to the 1 msec steady run time, the thermocouple did respond to both the first shock and record the second shock wave (at 22 msec). It recorded a maximum temperature of 702 R (390 K). The predicted temperature for this run was 1706.4 R (948 K). Owing to the short run time, transient temperature estimation technique 1 proved to be ineffective for this test run. Technique 2 didn't yield a definite value for the maximum temperature of the stagnant gas in the settling chamber of the nozzle, but, it did result in a range of temperatures within which the total temperature is expected to fall. This was because different time intervals between the measured temperature data points used for curve fitting produced different temperature curves and none of them actually matched the modified thermocouple response (most of them were pretty close to the modified thermocouple response). The range found was 1319.4 R -1800 R (733 K-1000 K). The predicted total temperature of 937 K falls within this range. The results of this technique are presented in Figs. 24 through 27.

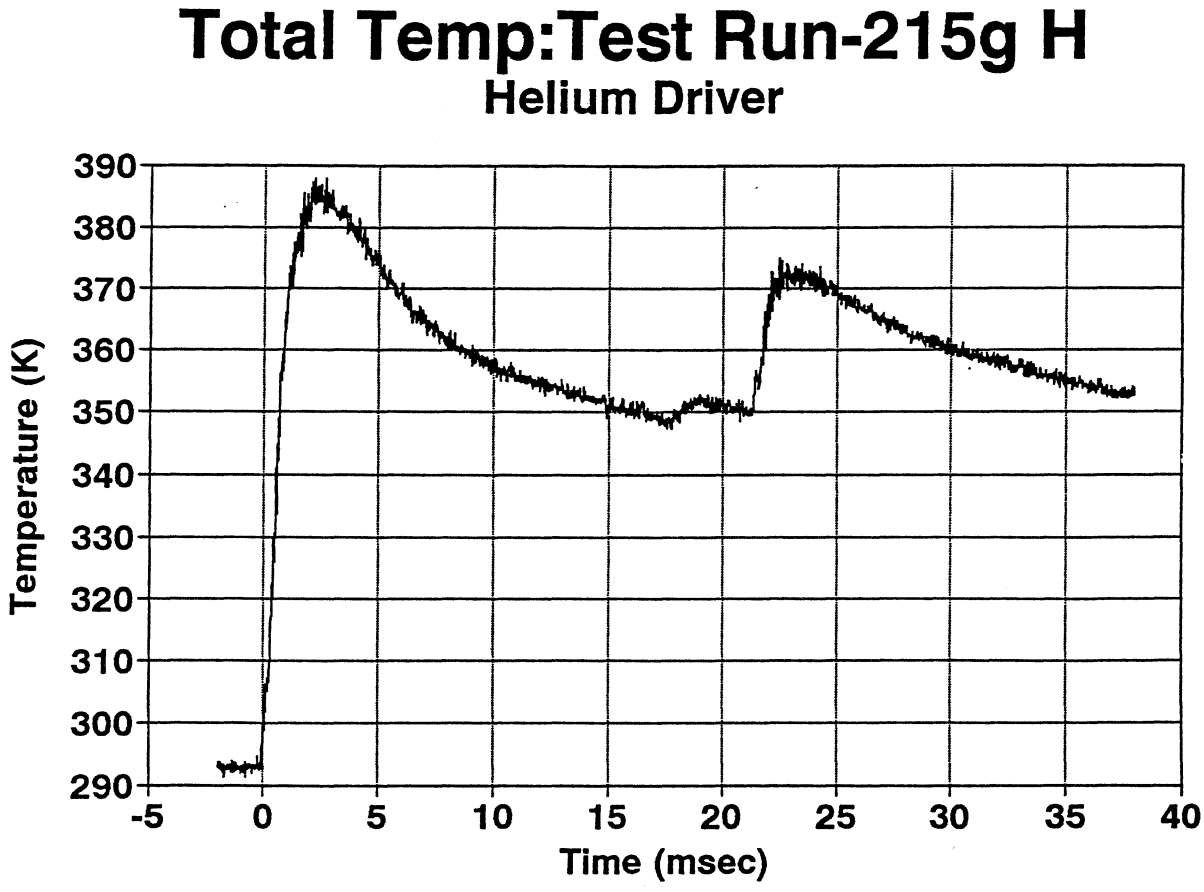

Figure 23 : Total Temperature Measurement With Helium Dr At 215 psig And 293 K

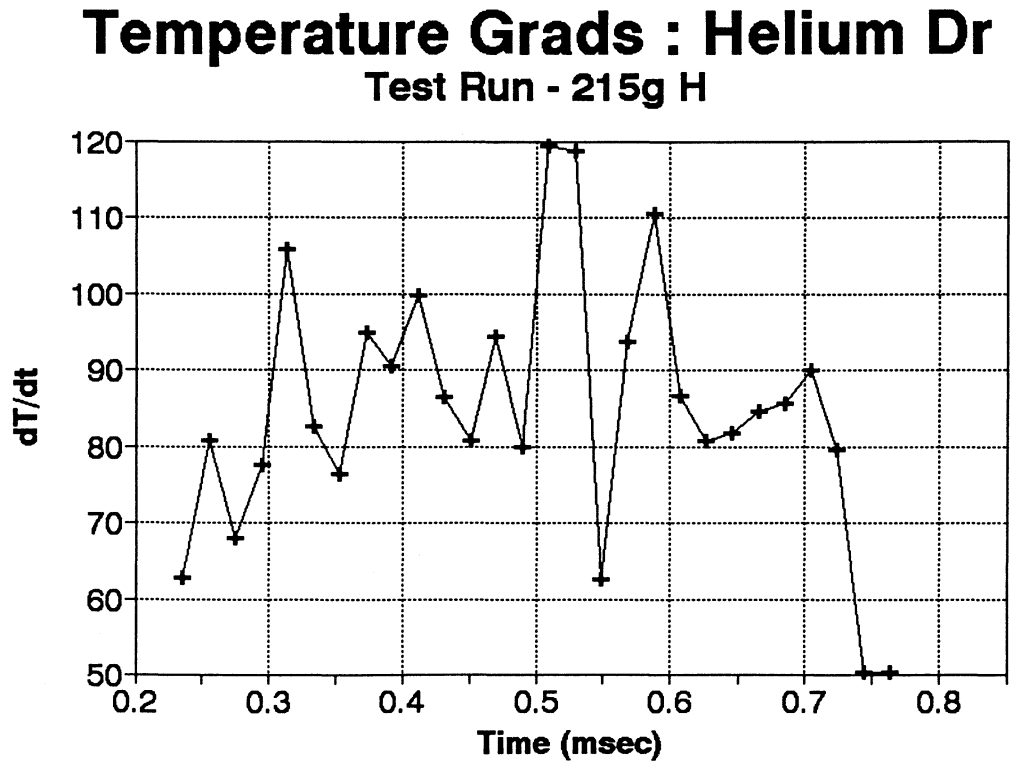

Figure 24 : Temp Derivatives For Test Run With He Dr At 215 psig, 293 K

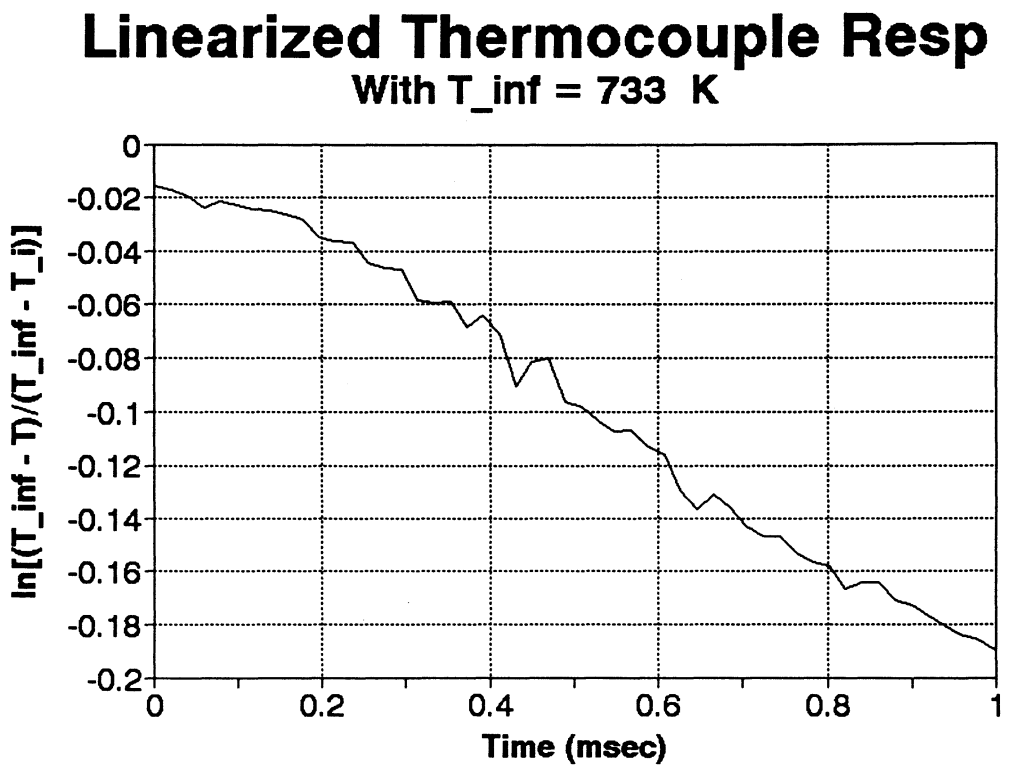

Figure 25 : Linearized Thermocouple Resp Test Run With He At 215 psig, 293 K

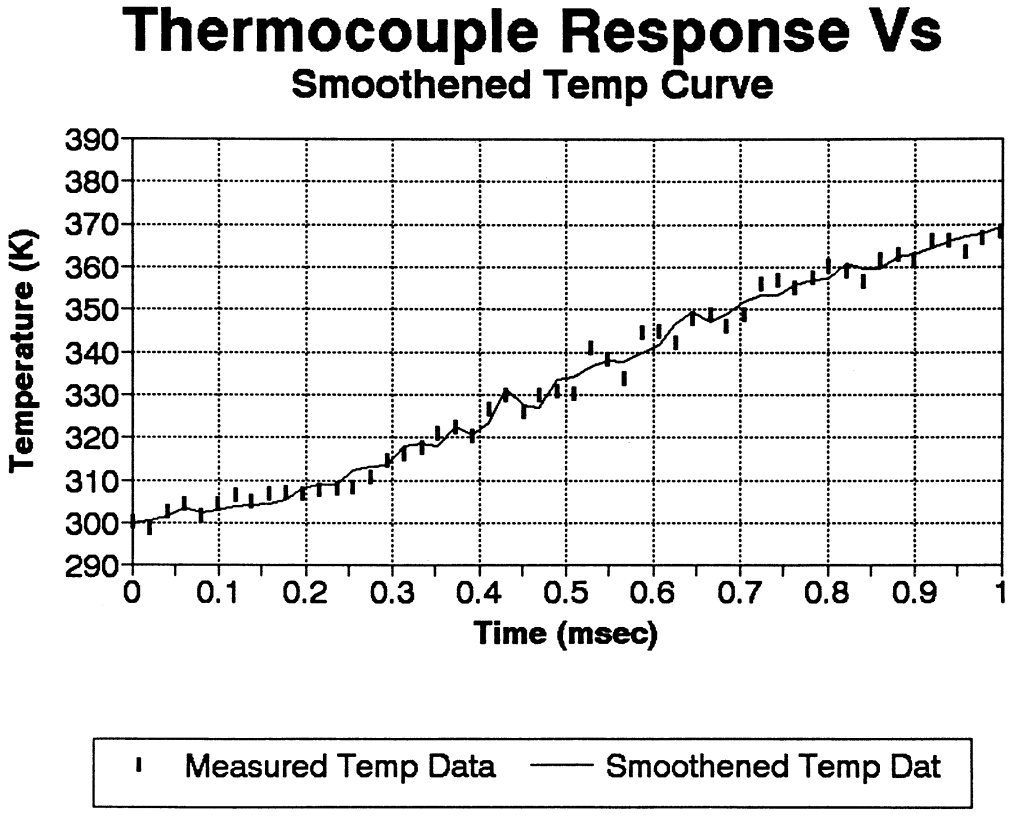

Figure 26 :Thermocouple Resp Vs Smoothened Temp Trace He At 215 psig, 293 K

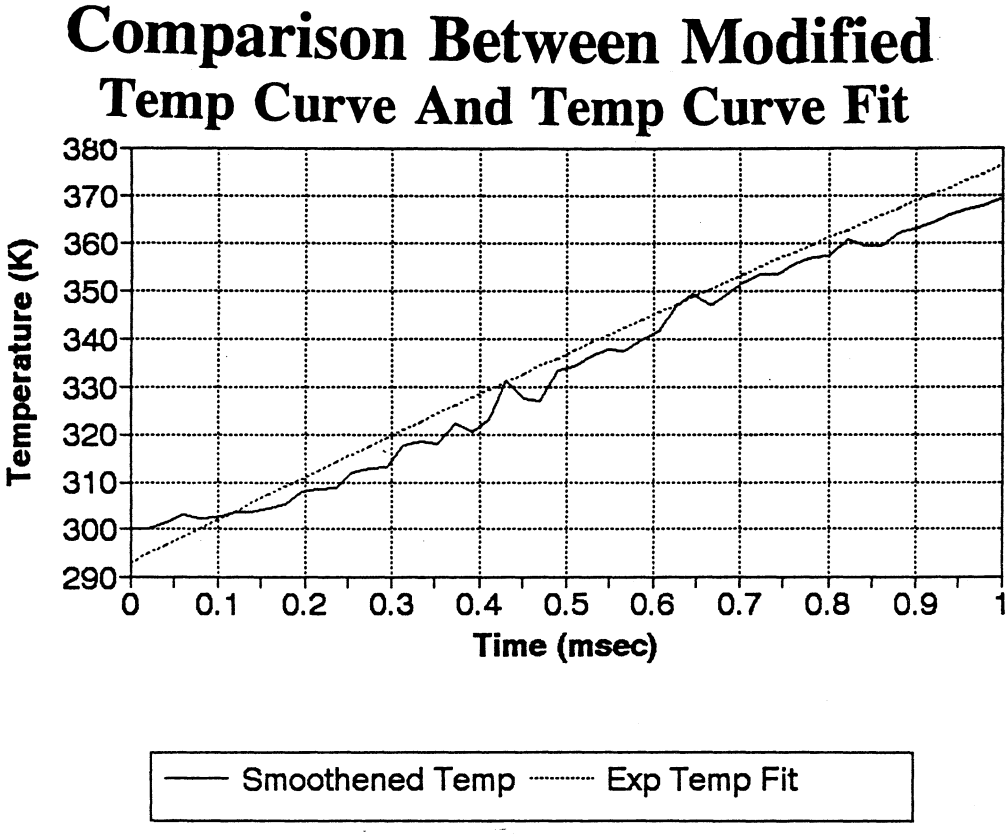

Figure 27: Modeled Temp (Technique 2)-Smoothened Temp He At 215 psig, 293 K

6.2.2 TEST RUN - 350g H

The test conditions for this test run were helium driver at 350 psig (2.414 MPa gage) and 163 R (293 K) driving into air at 13.65 psia (0.094 MPa) and 163 R (293 K).

The total pressure trace for this test run is given in Fig. 28. The predicted incident shock pressure for this case was 108.923 psia (0.7512 MPa) and the measured value was 120 psia (0.8276 MPa). This is rather peculiar and indicates that the incident shock wave is stronger than the predicted shock wave. The predicted reflected shock pressure was 489.6 psia (3.376 MPa), while the measured value was 400 psia (2.758 MPa). A second shock wave is recorded in this case as well, which occurs at 20 msec. The tiny pressure spikes at 15 and 34 msec are yet to be understood.

The static pressure trace at the nozzle exit is given in Fig. 29. The incident shock wave transmitted downstream at the throat as a pressure spike of 75 psia (0.5172 MPa). The pressure behind the incident shock wave as recorded in the total pressure measurement was about 120 psia (0.8276 MPa). Thus, it can be inferred that the modified incident shock wave transmitted through the throat is considerably weaker, by about 37.5%, than the incident shock wave transmitted into the settling chamber of the nozzle. The noise in the pressure trace at 3 msec is due to the external trigger that triggered the data acquisition for this measurement. The static pressure drops after about 3 msec and stays constant at approximately 4 psia (0.02758 MPa) for 12 msec. This long time duration is not exactly the run time, because the total pressure is decreasing

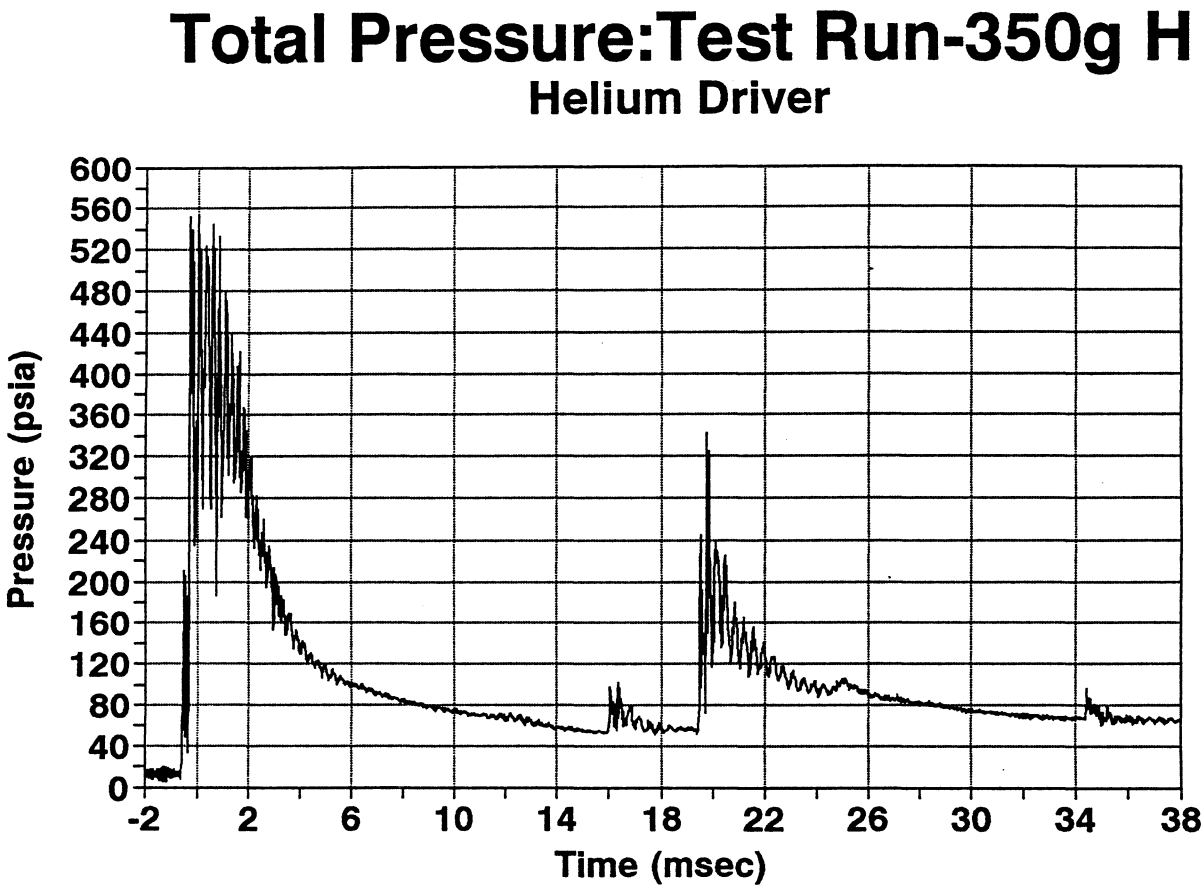

Figure 28 : Total Pressure Measurement With Helium Dr At 350 psig, 293 K

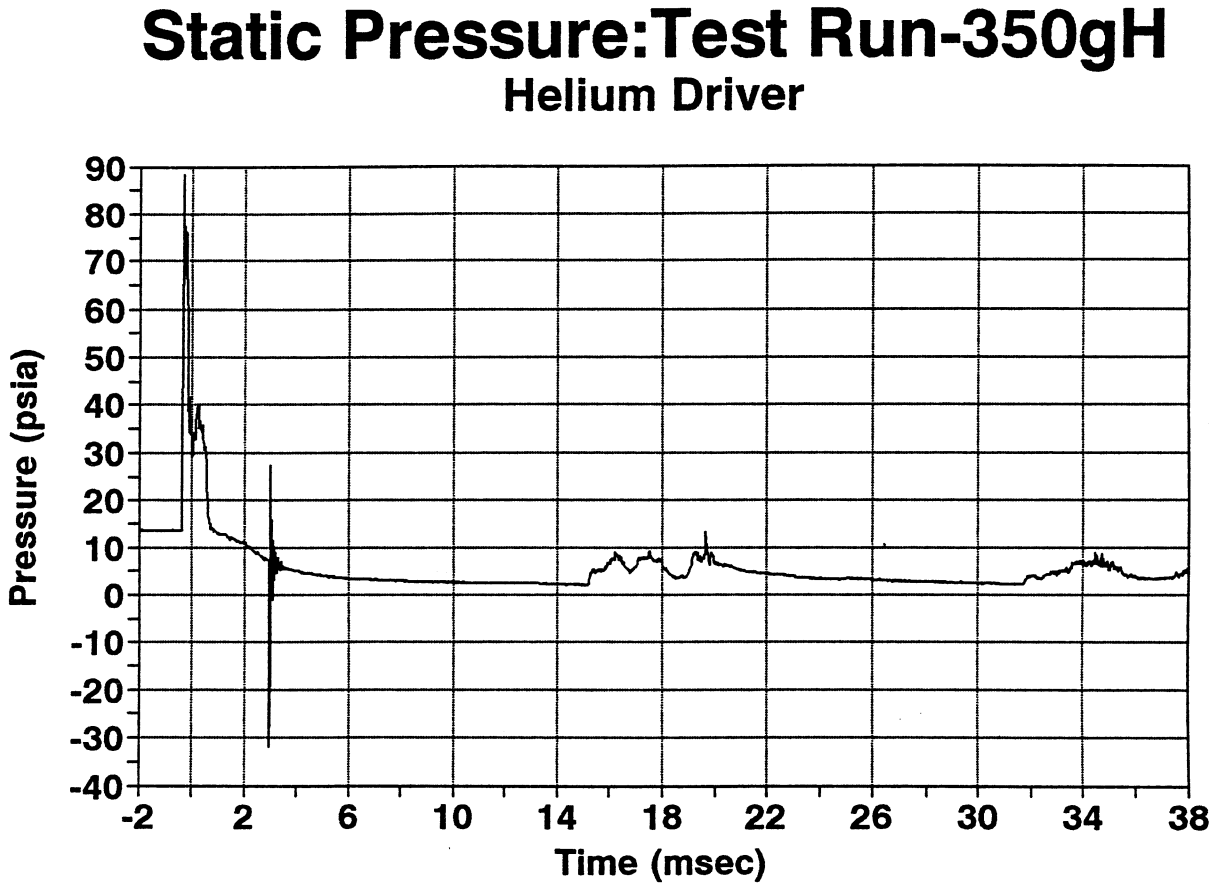

Figure 29 : Static Pressure Measurement With Helium Dr At 350 psig, 293 K

during this time. However, the nozzle remains started and produces supersonic flow until all the compressed gas is depleted. The properties of the gas mixture during this time are difficult to estimate and thus the measurements are difficult to interpret. The nozzle unstarts after approximately 14.5 msec. This is observed as an increase in the static pressure. The second shock wave recorded in the total pressure trace at 18.5 msec is responsible for the nozzle starting a second time. This appears as a drop in static pressure from 18.5 msec to 14 msec. The helium pressure traces, which have been obtained by using the non-flush diaphragm Lucas Schaevitz pressure transducer, are a little difficult to interpret. It was suspected that the wringing evident in the helium total pressure traces was due to the vibration of the pressure transducer at its natural frequency. To investigate this the pressure transducer was excited using a shaker table. The transducer was powered by a strain gage signal conditioner and the corresponding output was recorded. The frequency response function of the transducer output yielded natural frequencies of 10, 11, and 14 kHz. However, the wringing in the total pressure traces has a frequency of 2.75 kHz. Hence, it was concluded that the source for the wringing in the pressure signal was not due to resonant vibration of the transducer body. Consequently, the reason for the oscillations in the helium total pressure traces is yet to be investigated.

In all the test runs the effect of contaminated test gas due to the presence of debris like "pieces of Mylar" is yet to be investigated. In the case of helium test runs the reflected rarefaction head arrives in the settling chamber before the starting of the nozzle.

This results in a test gas which is a mixture of both air and helium and of unknown properties. Owing to the high stagnation temperature the calorically perfect gas assumption fails and the γ of the test gas is difficult to determine. This makes it difficult to predict the stagnation and free-stream properties in the case of helium test runs.

Table 2 : Summary of Helium Runs

VARIABLE	TEST RUN - 215g H		TEST RUN - 350g H	
	Measured	Predicted	Measured	Predicted
p_2	80 psia	84.547 psia	120 psia	108.923 psia
p_5	250 psia	336.634 psia	400 psia	489.597 psia
T_5	733-1000 K	948 K	*	1154.696 K
P_{static}	2.5 psia (avg)	11.059 psia	2 psia (avg)	16.0841 psia
M_s	2.2729	2.3349	2.5342	2.64245

* Unavailable

CHAPTER 7

RESULTS AND DISCUSSION - SURFACE MEASUREMENTS

7.1 SKIN FRICTION: A BRIEF OVERVIEW

Consider the simple case of the one dimensional fluid flow over a flat plate. The fluid layers adjacent to the wall are slowed down and travel at a velocity which is lower than that of layers above them. This is due to the viscosity of the fluid. These viscous effects diminish in magnitude as the vertical distance above the plate keeps increasing. After a certain distance this effect is practically negligible. Boundary layer analysis, terms this zone in which the viscous effects of the fluid are felt as the hydrodynamic boundary layer. The wall shear stress is given by

$$\tau_w = \mu \frac{\partial u}{\partial y} \qquad (26)$$

Where τ_w is the wall shear stress, and $\partial u/\partial y$ is the velocity gradient at the wall. The corresponding skin friction coefficient is given by the expression

$$C_f = (2\tau_w / \rho\, u_\infty^2) \qquad (27)$$

7.2 SKIN FRICTION BALANCE

The results of the skin friction measurements in the shock tunnel made by Dr. K.M.Chadwick of the department of Aerospace and Ocean Engineering of Virginia Tech are shown for comparison with the surface heat flux measurements.

This skin friction balance is based on the principle of a floating head attached to the end of a cantilever beam. When the floating head is subjected to a flow the corresponding shear force deflects the head producing a bending moment in the beam. Semiconductor strain gages are mounted on the sides of this cantilever beam at the base and sense the local strain when the beam deflects. The strain gages used with this balance are manufactured by Micro Gage Inc and have a resistance of 350 Ω and a gage factor of 135. Sketches of the cantilever beam and its housing are shown in Fig. 30. The skin friction balance, which was made of Ultem, was statically calibrated by hanging weights. In this procedure known weights are tied to a string, the other end of it being glued to the sensing or floating head. These weights can be so attached that the force applied to the sensing head is purely tangential, thus simulating a shear force. Consequently, this balance is a direct shear force measuring device. The calibration gave a sensitivity of 1.015 $mV/N/m^2$.

7.3 SKIN FRICTION MEASUREMENTS

The skin friction balance was inserted into the flat bottom plate at the exit of the Mach 3 nozzle where the flow Mach number was 2.87. The wall shear stress

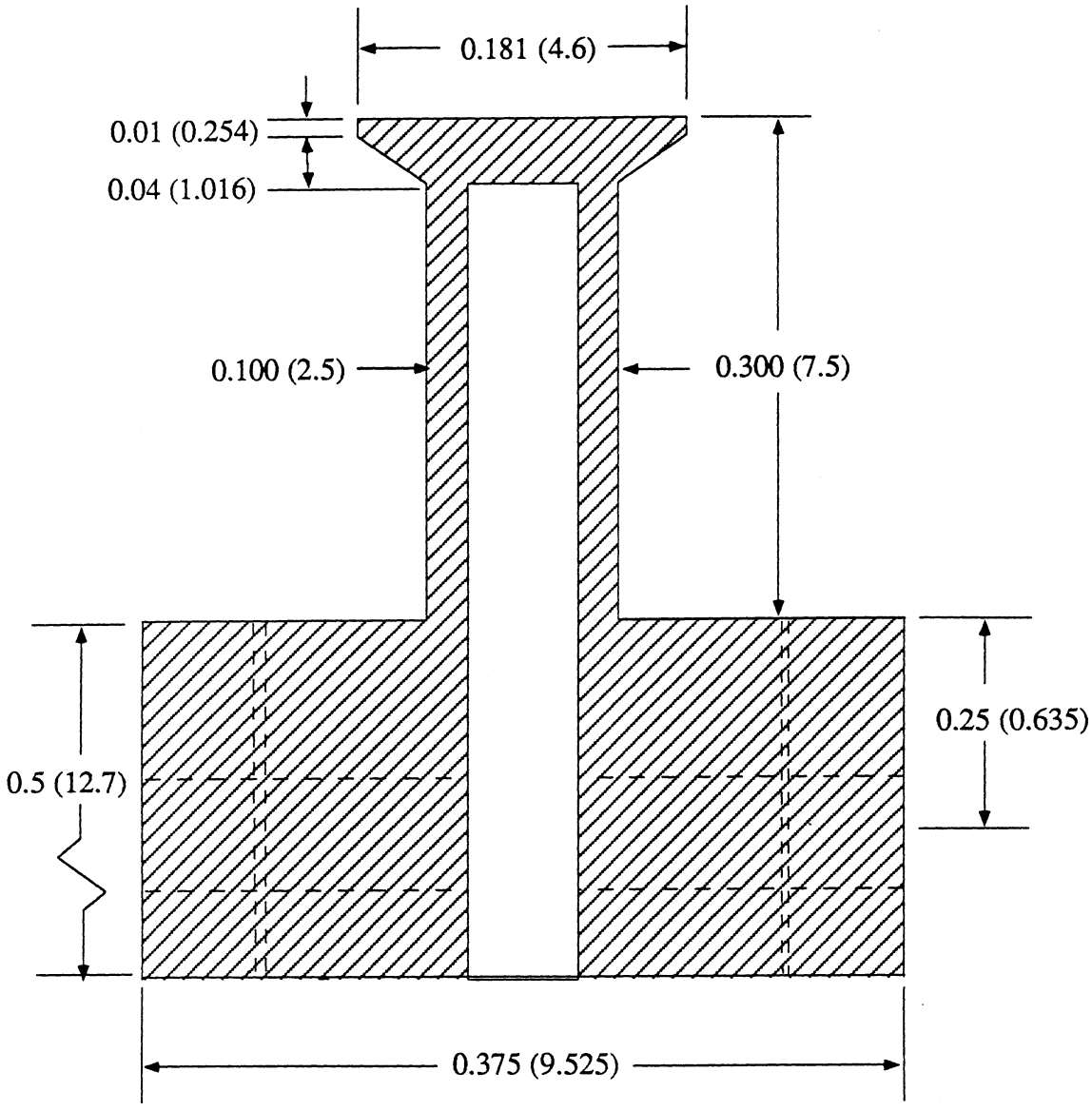

Side View

Figure 30a : Skin Friction Balance (Chadwick, 1992)

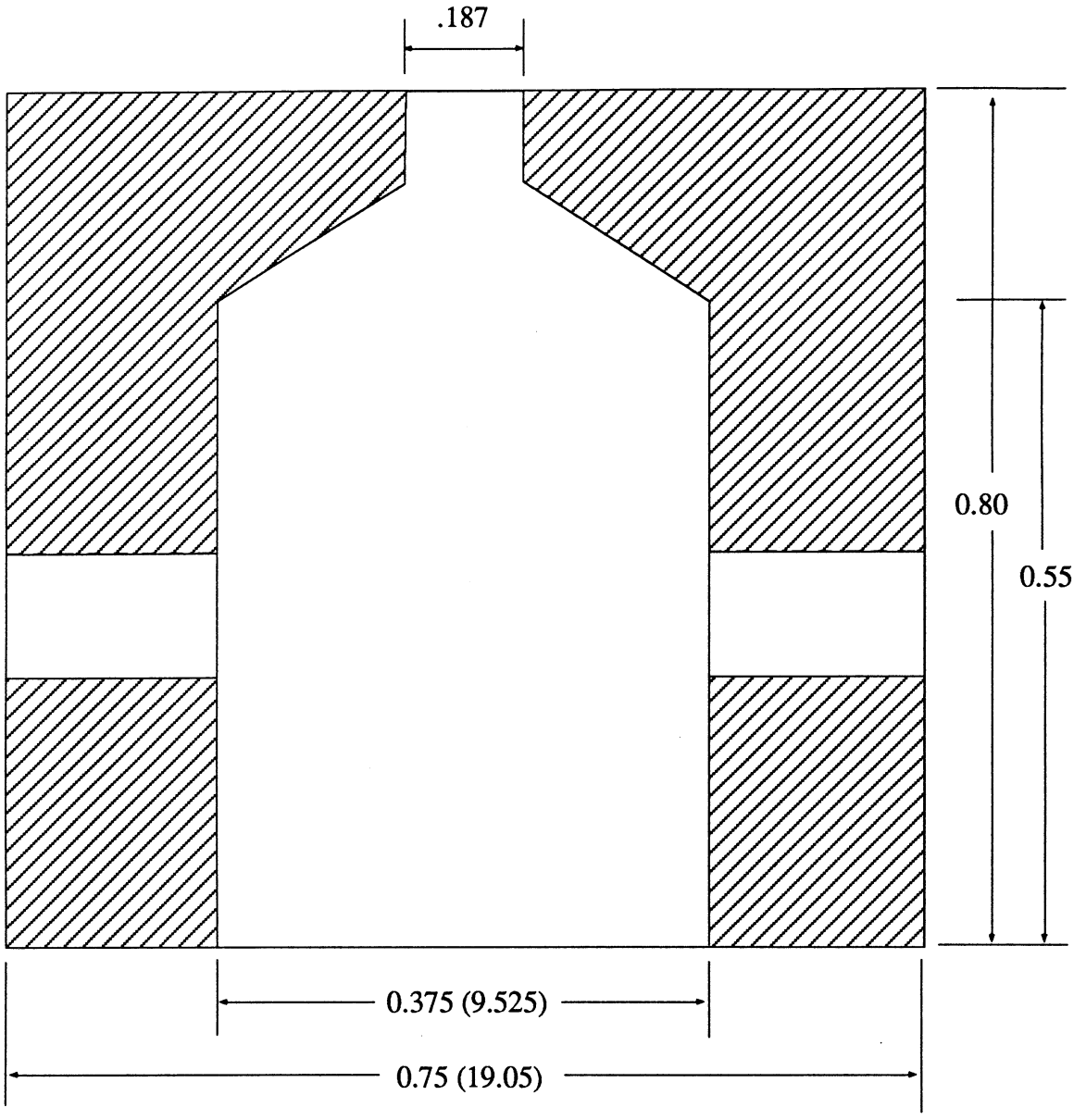

Side View

Material: Ultem
Units: inch (mm)

Figure 30b : Housing of the Skin Friction Balance (Chadwick, 1992)

measurements were conducted both for the air and helium drivers. The wall shear stress for an air driver at 200 psig (1.378 MPa g) and 527 R(293 K) driving into air at 13.65 psia (0.094 MPa) and 527 R(293 K) is given in Fig. 31. From Fig. 31 it is clear that the wall shear stress, (as soon as the nozzle starts) shoots up to an average value of about 750 pascal, and stays constant at this approximate value for about 6-7 msec. The steep spikes evident from the trace are attributed to the starting transients. As soon as the nozzle "unstarts" itself, there is again a sudden jump in the shear level (after about 25 msec). The reason for this has yet to be confirmed. This skin friction measurement is made in a decreasing total and static pressure test condition.

Another wall shear stress measurement was made using a helium driver at 200 psig (1.438 MPa g) and 527 R (293 K) driving into air at 13.65 psia (0.094 MPa) and 527 R (293 K). The wall shear trace is given in Fig 32. After the starting transients, the shear stress increases to an average constant value of 650 pascal. This is constant for about 2 msec, the duration for which the total pressure is also constant, and then starts decreasing. The response again shoots up as soon as the nozzle unstarts. The skin friction balance picked up the second shock wave after 22 msec, which is the same time when second shock wave is recorded in the corresponding total and static pressure traces. Owing to the uncertainties involved in the total pressure and total temperature measurements for the test runs with helium drivers it is difficult to interpret these skin friction measurements. This difficulty is further complicated by the fact that the test gas during this time is a mixture of helium and air of unknown proportion and properties.

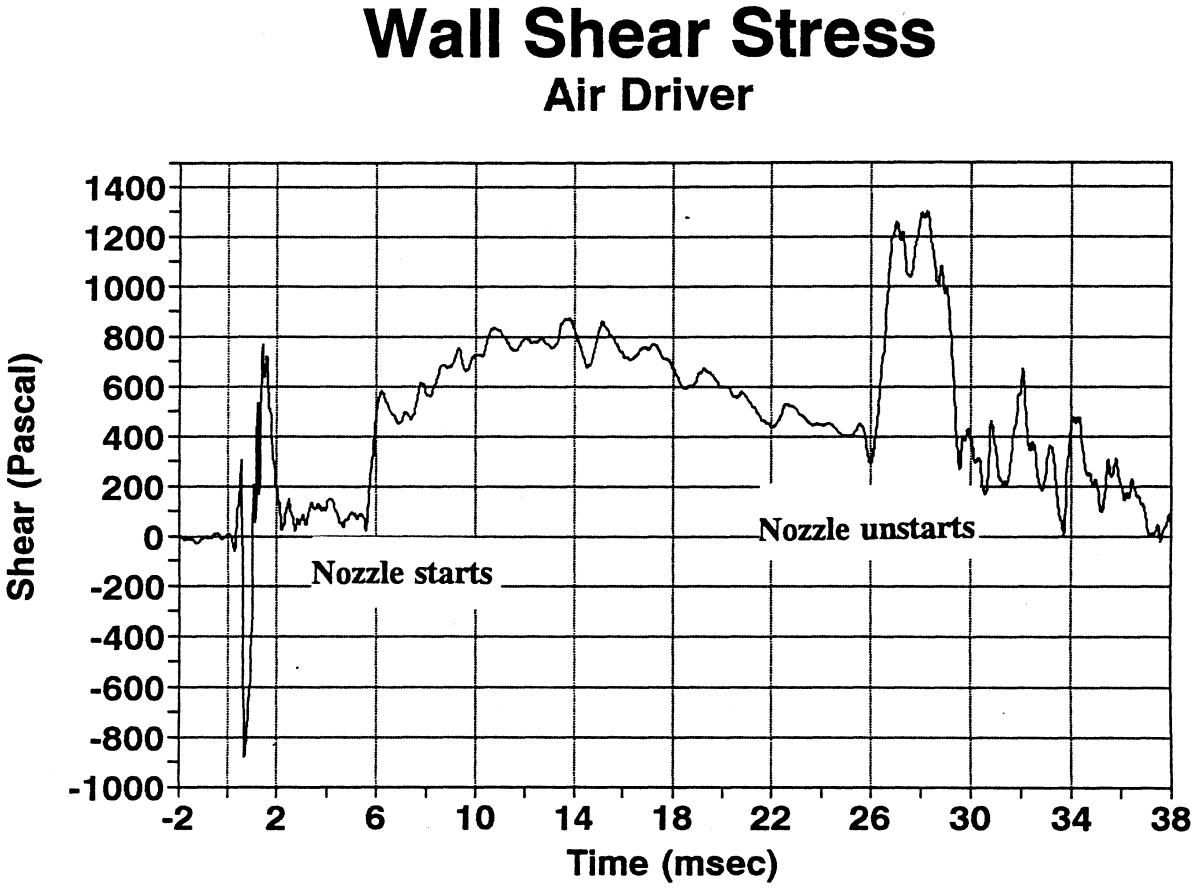

Figure 31 : Wall Shear Stress measurement with air driver at 200 psig, 293 K

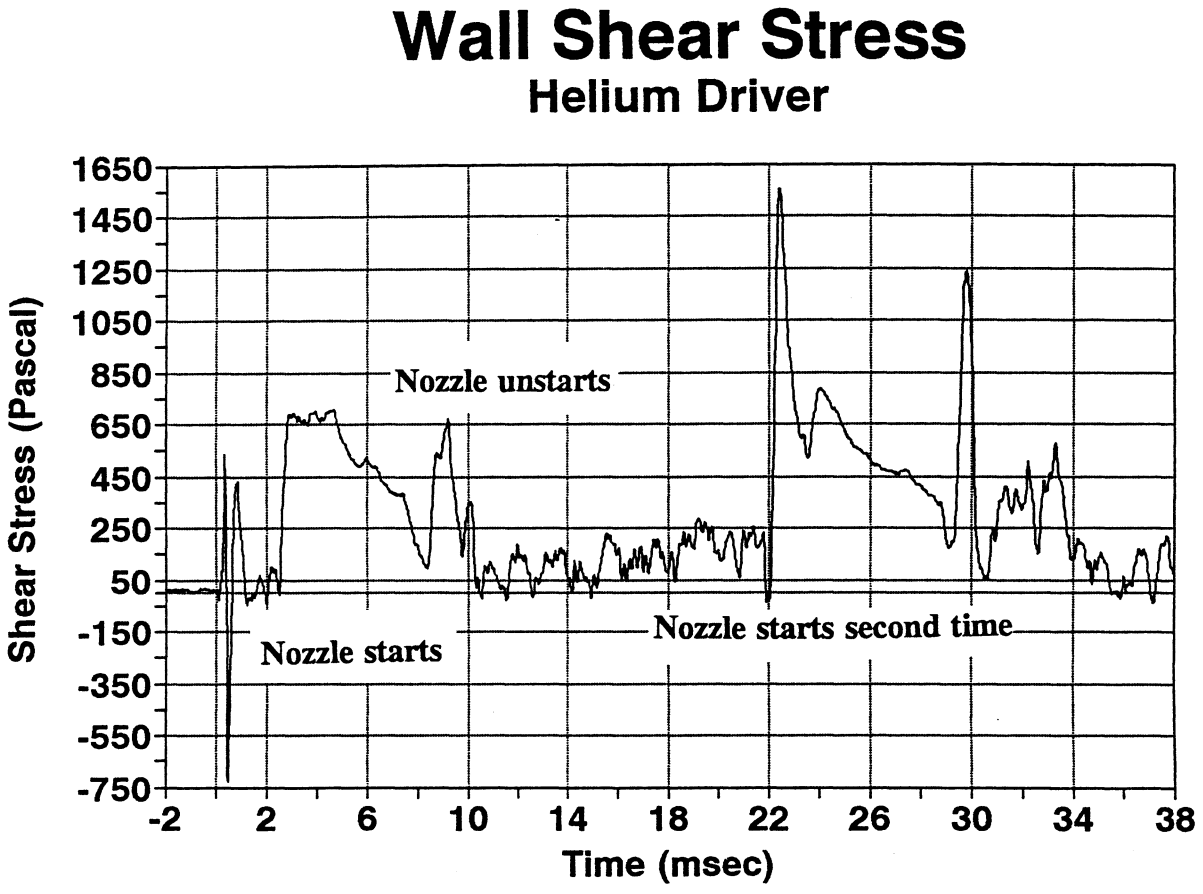

Figure 32 : Wall Shear Stress with He Dr At 200 psig, 293 K

7.4 SURFACE HEAT FLUX MEASUREMENTS IN THE NOZZLE

The heat flux microsensor patented by Profs. T.E.Diller and S.Onishi of Virginia Tech was used in making heat flux measurements at the exit of the nozzle. Figure 33 shows a portrait of the microsensor. The microsensor is a direct heat flux and surface temperature measuring device and consists of a series of thermocouples forming a differential thermopile. The output voltage from this differential thermopile is directly proportional to the surface heat flux. More details concerning the design and operation of the heat flux microsensor are presented by Hager et al. (1991).

A surface heat flux measurement was made at the nozzle's exit using an air driver at the test conditions of test run 200g A and the corresponding trace is given in Fig. 32. As soon as the nozzle starts the surface heat flux jumps up to about 7.5 W/cm^2. It stays constant at this level until 12 msec after which time it is predicted that the contact surface enters the settling chamber of the nozzle leading to a drop in the total temperature of the flow and hence the surface heat flux at the nozzle's exit. The heat flux signal becomes difficult to interpret after 24 msec, i.e, after the nozzle unstarts. In order to interpret the correlation between the surface heat flux and skin friction measurements at the exit of the nozzle the Stanton number and skin friction coefficient were calculated. The Stanton number was calculated using the expression

$$St = \frac{Nu}{Re\ Pr} \tag{28}$$

where Re is the local free-stream Reynolds number given by Re= ρ u x/μ, Pr for the test gas of Air has been taken to be 0.7. Nu, the Nusselt number is given as Nu = hX/K. The local convective heat transfer coefficient h is

$$h=\frac{q''}{T_{aw}-T_w} \tag{29}$$

where T_w is the wall temperature and q" is the surface heat flux. T_{aw} is the adiabatic wall temperature and is calculated by

$$T_{aw}=T_\infty\left[1+\frac{rM^2(\gamma-1)}{2}\right] \tag{30}$$

where the recovery factor r = $Pr^{1/3}$. All the fluid properties were calculated at temperature of 400 K which is the average of T_{aw} and T_w. The local sound speed at the nozzle's exit was calculated at the local free-stream temperature of 222 K. The local skin friction coefficient was calculated using Eq. 27.

C_f /2 and Stanton number for test run 200g A are plotted in Fig. 35. The skin friction coefficient and Stanton number follow the Reynold's analytical relation, C_f /2 = St to within 50% during the steady run time of the nozzle, i.e, from about 6 msec to 12 msec. From Fig. 35 it is clear that although the nozzle starts at about 4 msec, the skin friction transducer doesn't record an appreciable rise in skin friction level while the heat flux microsensor detects an abrupt increase in heat flux. This has been attributed to the relatively slow response of the skin friction sensor compared to that of

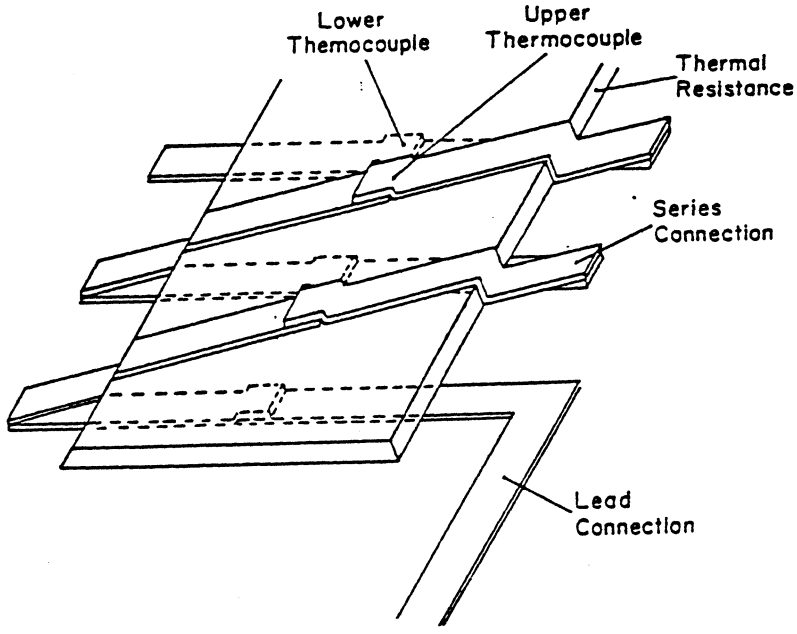

Detailed section of microsensor

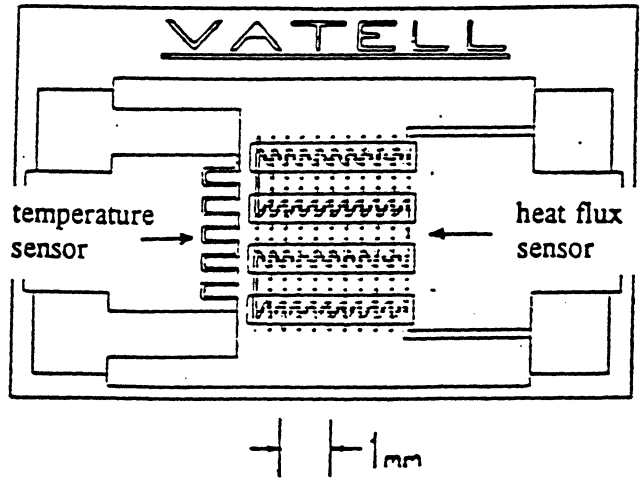

Microsensor with surface
resistance thermometer

Figure 33 : Schematic of The Heat Flux Microsensor (Hager et al., 1991)

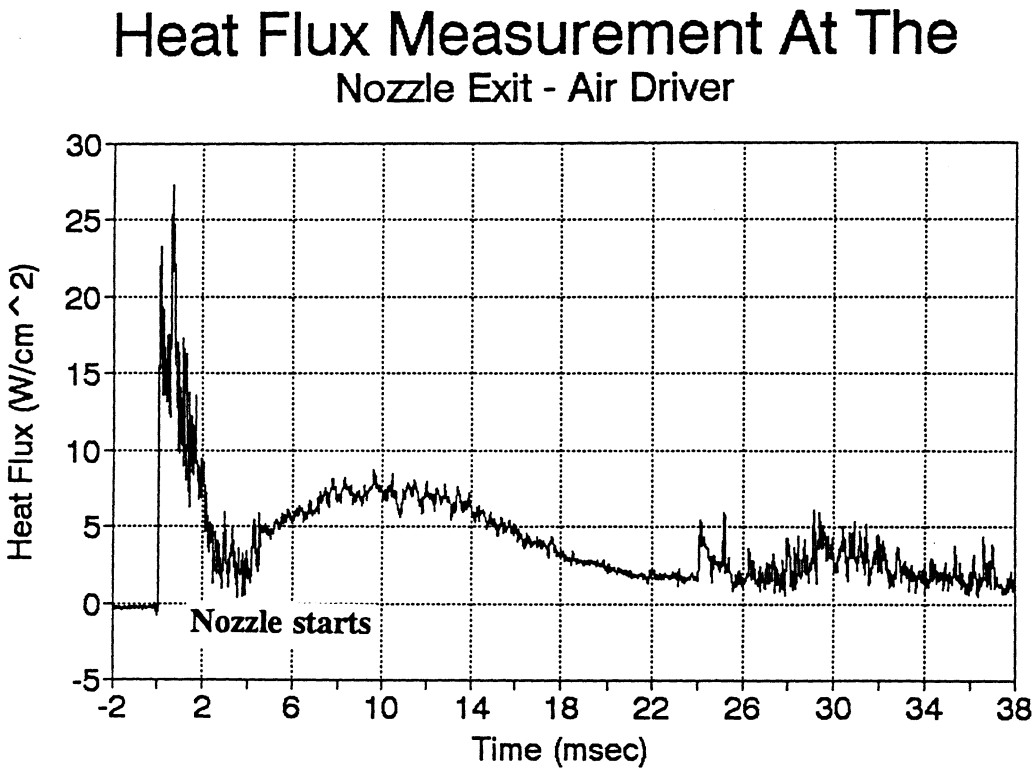

Figure 34 : Heat Flux Measurement (Nozzle Exit) Air Dr At 200 psig, 293 K

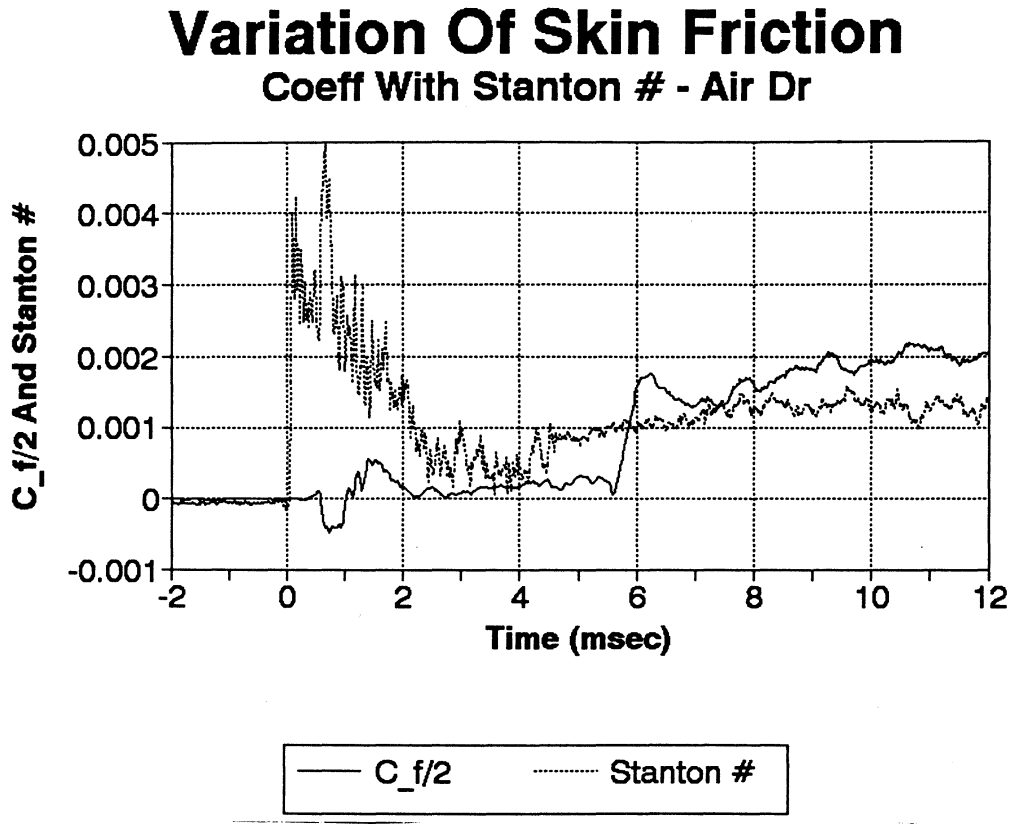

Figure 35 : Skin Friction Vs Surface Heat Flux With Air Dr At 200 psig, 293 K

the heat flux microsensor. Also, the starting transients have been recorded as significant heat flux levels by the heat flux microsensor while the skin friction transducer's output is almost zero. This can be explained due to the fact before the nozzle starts the flow is subsonic and hence the wall shear stress is negligible. However, the subsonic fluid does have a free-stream temperature (close to the total temperature) which is higher than the local wall temperature resulting in appreciable wall heat flux. Once the nozzle starts and the flow becomes supersonic the free-stream temperature drops way below the total temperature and the so does the corresponding heat transfer to the wall. It is also obvious that Reynold's analogy doesn't apply when the flow is unsteady or has shocks.

CHAPTER 8

CONCLUSIONS AND RECOMMENDATIONS

8.1 Conclusions

The primary objective of building a shock tunnel that produced a high temperature supersonic flow for a short duration has been successfully achieved. The nozzle of the shock tunnel was successfully instrumented to record the pressures and temperatures in the flow. Flow The unsteady starting process of the shock tunnel nozzle has been successfully established. Test runs were successfully made with an air driver at different driving pressures. The total and static pressure results for the air runs coincided remarkably well with the expected values. The air driver produced supersonic Mach 3 flow for run times that were longer than expected. Thermocouples were successfully fabricated to measure the total temperature in the flow for the air driver tests. Two first order transient temperature fit techniques were successfully utilized to estimate the total temperature in the flow for both air and helium runs. Both the techniques were successful in predicting the total temperature in case of the air runs. The second technique which involved using the temperature derivatives, was developed especially to estimate the total temperature from the measured helium temperature data. Incident

shock strength measurements for both the air and helium drivers compared very well with the expected values indicating that the phenomenon of shock attenuation was not a major problem. Total pressure, total temperature and static pressure measurements for the helium driver proved to be moderately successful. There were some problems in interpreting the total pressures and it was difficult to establish the maximum temperature in the flow for helium driver tests.

The heat flux microsensor was successfully tested using air driver. The heat flux results for the air test runs were successfully compared with the skin friction results. The skin friction coefficient and the Stanton number followed the Reynold's analogy to within 50% during the steady run time of the tunnel. It can also be concluded that the shock tunnel proved to be a convenient device for testing the transient response of the high frequency surface transducers like the heat flux microsensor.

8.2 Recommendations

To produce higher enthalpy supersonic flows in the shock tunnel using a helium driver the following recommendations are suggested.

1. In order to minimize the starting time for the nozzle it is suggested that the length of the settling chamber be made as small as possible or to start directly from the throat making the nozzle to be a simple divergent nozzle.

2. Another technique to eliminate the formation of these complex waves is place a

second diaphragm at the entrance of a diverging nozzle attached to the shock tunnel. In this case the incident shock wave breaks the second diaphragm and the gas behind it is accelerated in the nozzle. The incident shock wave itself is completely reflected back into the tunnel. This may eliminate the unsteady waves produced in the current nozzle.

3. Since the air tests have been proved to be successful, it is recommended that the driven section of the tunnel be evacuated. Thereby, for the normal driving pressure of 200 psig (1.379 MPa gage) a stronger shock wave is produced resulting in higher stagnation temperature conditions.

4. To make the interpretation of the helium total pressure measurements more easier it is recommended that a faster responding pressure sensor (preferably a silicon diaphragm flush mount sensor) be utilized. Either faster responding thermocouples or optical techniques better techniques have to be employed for measuring the total and free-stream temperatures in the flow for helium driver tests.

5. It is recommended that the driving gas be heated. For a given driving pressure a heated driving gas results in a higher sound speed and hence a stronger shock and larger stagnation conditions.

6. It is suggested that a series of shadowgraphs be taken at different times to clearly establish the wave patterns in the nozzle at different positions and times. This would be added tool in the interpretation of the pressure and temperature measurements.In order to improve the run time, the tailored interface method can be adopted.

REFERENCES

ASME, 1956, "ASME Handbook Engineering Tables".

ASTM, 1981, "Manual on the use of Thermocouples in Temperature Measurement", ASTM Special Technical Publication 470B.

Amann, H.O., and Reichenbach, H., 1973, "Unsteady Flow Phenomena in Shock Tube Nozzles", Proceedings of the Ninth International Shock Tube Symposium, Stanford, MA.

Anderson, J.D., 1990, "Modern Compressible Flow with a Historical Perspective",.

Breggren, R.E., Compton, D.L., Canning, T.N., and Page, W.A., 1969, "Ames High Explosive-Facility Shock-Tube Facility", Proceedings of the Seventh International Shock Tube Symposium.

Chadwick, K.M., 1992, "An Actively Cooled Floating Element Skin Friction Balance for Direct Measurement in High Enthalpy Supersonic Flows", Ph.d Dissertation, Blacksburg, VA.

Diller, T.E., Hager, J.M., Langley, L.W., Onishi, S., Simmons, S., Smith, D., 1991, "Experimental Performance of A Heat Flux Microsensor", Journal of Engineering for Gas Turbines and Power, Vol 113.

Diller, T.E., Hager, J.M., Langley, L.W., Onishi,S., Terrell, J.P., 1991, "Measurements With The Heat Flux Microsensor", Proceedings of The 37th International Instrumentation Symposium.

Dvir, M., Low, W., Stricker, J., and Maniv, S., 1965, "Interaction of Shock Waves with Taper Sections", Proceedings of the Fifth International Shock Tube Symposium.

Gaydon, A.G., and Hurle, I.R., 1963, "The Shock Tube in High Temperature Chemical Physics".

GASL, 1990, "Shock Tunnel Report", GASL TM236, Rockonokoma, NY.

Hewlett Packard, "3562A Dynamic Signal Analyzer", Operating Manual.

Hildebrand, F.B., 1956, 1974, "Introduction To Numerical Analysis".

Incropera, F.P., and Dewitt, D.P., 1985, "Fundamentals of Heat and Mass Transfer".

Kreyzig, E., 1983, "Advanced Engineering Mathematics".

Kulite Semiconductor Products, "Kulite Miniature IS Silicon Diaphragm Pressure Transducer Catalog", Leonia, NJ.

Measurements Group Inc, Instruments Division, "2310 Strain Gage Conditioner Catalog".

NOLAND, 1949, "Industrial Supplies-Machinery Catalog".

Omega Engineering Inc, Complete Temperature Measurement Handbook and Encyclopedia, Vol 28.

Shapiro, A.H., 1954, "The Dynamics and Thermodynamics of Compressible Fluid Flow", Vol 2.

Witliff, C.E, Wilson, M.R., and Hertzberg, A., "The Tailored Interface Hypersonic Shock Tunnel".

Zucrow, M.J., and Hoffman, J.D., 1977, "Gas Dynamics Multidimensional Flow", vol 2.

APPENDIX A

SHOCK TUNNEL INSTRUMENTATION

A.1 PRESSURE SENSORS

The pressures, both total and static, in the flow of a shock tunnel can be measured by a variety of pressure transducers. The most commonly used pressure transducers are either the active strain gage type or piezo- electric type.

In the active strain gage type transducers, a full wheatstone bridge consisting of four miniature strain gages is directly diffused onto a miniature metal or silicon diaphragm. This miniaturization imparts a very high frequency response to the sensor. This diaphragm, when exposed to a pressure or stress produces an unbalance in the otherwise balanced wheatstone bridge. This bridge unbalance is then recorded as a voltage output. Strain gage pressure transducers come in a variety of pressure ranges. They are usually compensated for temperature, and vibration effects. They also come in different ranges of frequency responses, starting from about 25 khz to about 500 khz. The main disadvantage in using them is that they are very susceptible to extraneous particulate matter in the flow. Although they come with protective screens (like in the case of Kulite transducers), they can still be damaged by particles traveling at supersonic

speeds.

A Kulite semi-conductor strain gage , 0-150 psi(1.034 MPa) range, differential pressure transducer was inserted in one of the side plates of the settling chamber to measure the stagnation pressure or the reservoir pressure in the nozzle. The particular transducer used, an XT-190-150 model transducer, measures the gage pressure. This transducer is equipped with a temperature compensation module which facilitates the operation of the transducer in the temperature range of 80 F (26.66 C) to 180 F (82.22 C). It has a frequency response of 175 khz and has an over-range pressure of 300 psia (2.069 MPa). It has a burst pressure of 900 psia (6.207 MPa). It is a voltage mode transducer and can take an excitation voltage ranging between 5 to 15 volts dc. It has a sensitivity of 0.871 mV/psi. The signal from this pressure transducer was relayed to channel 5 of the Ectron voltage amplifier set at a gain of 50. The static calibration of the transducer was performed on the same channel and at the same gain. Figure 34 shows the static calibration curve for this transducer as calibrated using a dead weight tester. The transducer exhibited a linear response even beyond the operating pressure limit of 150 psia(1.0345 MPa).

A kulite XCQ-062-50A pressure transducer of the same kind but of a lower pressure range, 0-50 psia (0.3348 MPa), was used to measure the free stream static pressure at the exit of the nozzle. It has a sensitivity of about 2.302 mV/psi, an over pressure of 100 psia (0.6896 MPa), and a burst pressure of 150 psia (1.0345 MPa) which is 3 times the rated pressure. The operating voltage is once again 10-15 vdc. The input

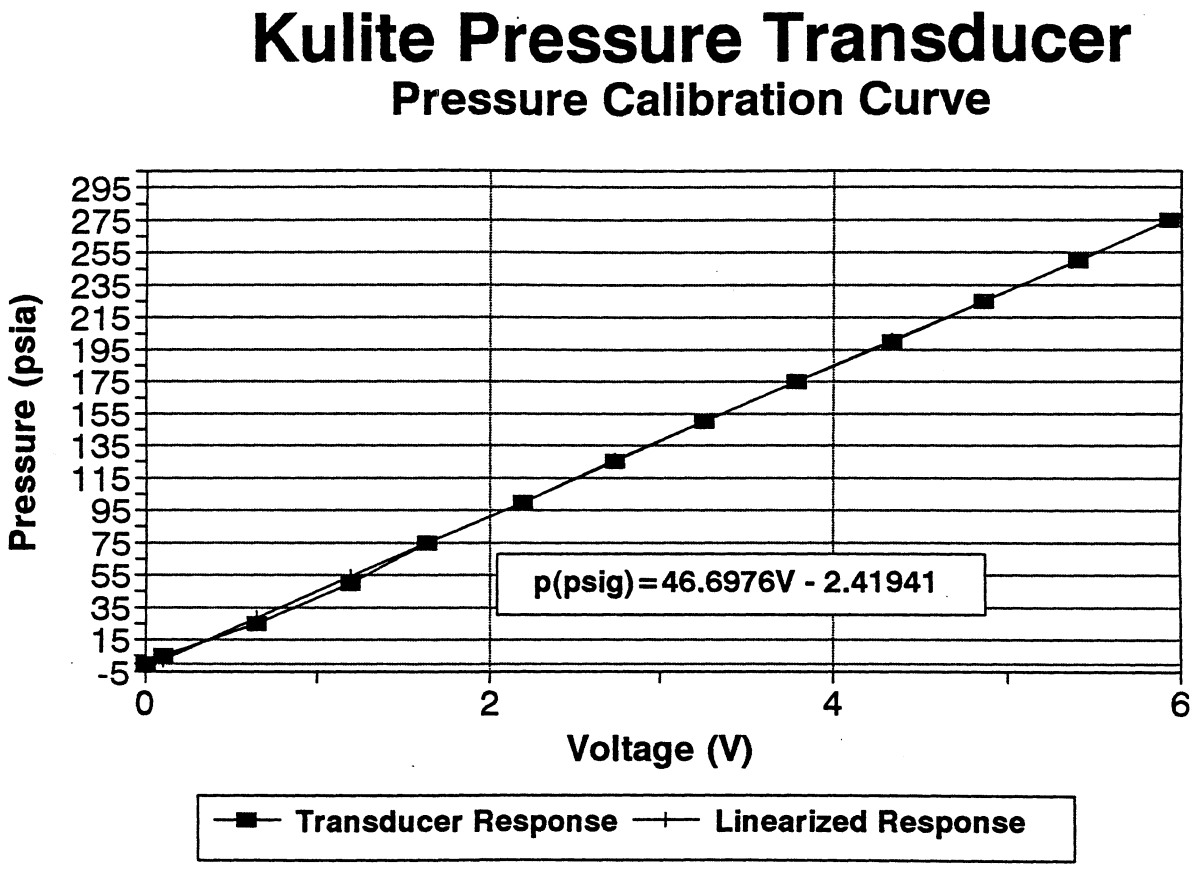

Figure 36 : Kulite Pressure Transducer Calibration

and output impedances are 1499 Ω and 1470 Ω respectively. The other pressure transducer that was used was a non-flush mount sensor. This pressure sensor, a P1200 series, high performance sensor manufactured by Schaevitz Engineering, is a 500 psi(3.448 MPa) vented gage transducer. It is extremely rugged and has a solid housing with a nut for mounting purposes. It also utilizes a diaphragm with strain gages mounted on it. However, unlike the Kulite transducer, this pressure sensor uses a flat beam which houses the strain gages. This beam is then stressed by a force rod that is directly exposed to the pressure media. Because of its non-flush mount sensing diaphragm, the response of the overall transducer is considerably slow. Also, owing to the recess between the sensing diaphragm and the surface, the signal is not as clean (due to the oscillating waves formed in this recess) and it can be more difficult to interpret the pressure signals. The static calibration curve for this transducer is given in Fig. 37.

A.2 VOLTAGE AMPLIFIERS

Voltage amplifiers were used to boost the signals from the pressure transducers and the skin friction sensors. The Ectron 6 channel voltage amplifier and the strain gage signal conditioner were used for this purpose. Some of the features of the ECTRON 500 series amplifier are given below. The ECTRON 500 series amplifier is a wide band, differential dc amplifier with direct coupling and high loop gains. This amplifier is totally isolated from the output and ground. It has variable gains ranging from 1 to 1000 with 1% accuracy. It can supply a bridge excitation voltage in two different ranges, 2.5-

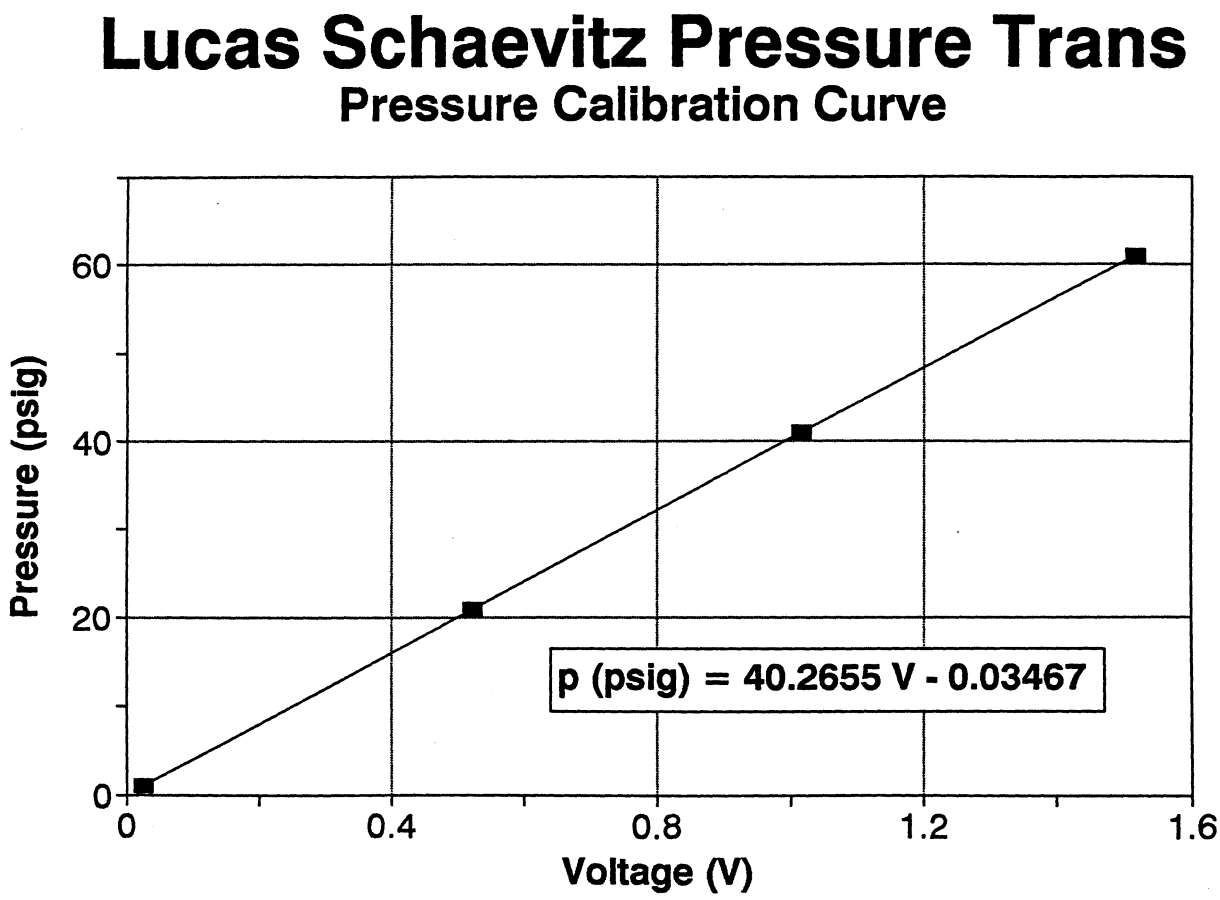

Figure 37 : Lucas Schaevitz Pressure Transducer Calibration

5 V dc, 5-15 Vdc. This amplifier can be used with strain gage devices with one, two or four active strain elements. When used in conjunction with one-quarter or one-half bridge strain gage devices, this amplifier can be balanced by using external resistors. Further, this amplifier comes with a balance control that can be used to balance the bridge at reference or quiescent conditions.

The 2310 Strain Gage signal Conditioning Amplifier manufactured by the Instruments division of the Measurements Group Inc, was used for amplifying the voltage signals from the skin friction sensor. This signal conditioner is a multi-channel system used for amplifying the low-level signals from strain gage devices. It operates on a bridge excitation ranging from 0.5 to 15 volts dc. It has a fully adjusted variable gain ranging from 1 to 11,000.

A.3 DATA ACQUISITION SYSTEM

Data for all the tests was acquired using the Hewlett Packard 3562 A dynamic signal analyzer. It is an FFT based, dual channel, dynamic signal analyzer with a measurement range of 64μ Hz to 100 khz. It has an accuracy of $\pm$ 0.004% of the frequency reading and a resolution of 1/800 of the total time or frequency span. The HP3562 A can be triggered externally by a voltage and it also has the capability to be pre-triggered. Pre-triggering allows data acquisition prior to the arrival of the trigger signal. It can be triggered from either channel and data is acquired simultaneously on both of them. The source for this triggering can also be an external source. The

HP3562 A also has the capacity to store data in its internal memory. A peripheral disc drive attached to it can be used to store data on floppy discs. The HP 3562 A has its own plotters that can plot the time domain traces. The data stored in this analyzer has to be converted in to its corresponding ASCII form before it can be used for processing with other software programs.

APPENDIX B

NUMERICAL PROGRAMS

A numerical program was written in FORTRAN 77 to calculate the expected flow properties in the shock tunnel. This program uses the fundamental shock tunnel equations given in chapter 4. These basic equations are based on the inviscid, perfect gas, constant specific heat assumption. For the given test conditions and tube lengths, the incident shock Mach number was first calculated by using an iterative technique. This technique involved assigning a guess value for the shock Mach number. This guess value was then used to compute the diaphragm pressure ratio for the given tube lengths using Eq. 13. This computed diaphragm pressure ratio was then compared to the actual diaphragm ratio for the given test gas pressures, and iteration was continued until the former value is within 1% of the latter. This shock Mach number was then inserted into the basic shock tunnel equations to obtain the pressures, temperatures the flow speeds and the run time.

Another program was written in FORTRAN 77 to calculate the modified 2 data points for the measured temperature data. This program uses Eqs.22 through 24 to obtain a smooth curve fit for the measured data that still retains all the important trends of the measured temperature trace. The program then uses these modified data points and calculates the center temperature derivatives using the numerical form of Eq. 25.

```
C-------------------------------------------------------------

C       PROGRAM TO CALCULATE GAS PROPERTIES IN THE SHOCK TUNNEL

C-------------------------------------------------------------
C
C
C
C
C
C
C-------------------------------------------------------------

C                            INPUT PARAMETERS

C-------------------------------------------------------------
        REAL MM1,MM4,PR,M,M3,M2,P1,P4,NOMTIM ,PRATIO,P5,P2,P3
        OPEN(1,FILE='B:RUN4.OUT')
        WRITE(*,*) 'INPUT DRIVING PRESSURE,DRIVEN PR,G4,G1'
        READ(*,20) P4
        READ(*,20) P1
        READ(*,20) G4
        READ(*,20) G1
20      FORMAT(F10.9)
        WRITE(*,*) 'INPUT DRIVING GAS TEMP,DRIVEN GAS TEMP'
        READ(*,30) T4
        READ(*,30) T1
30      FORMAT(F10.5)
        WRITE(*,*) 'INPUT MOLMASS OF DRIVING GAS,MOLMASS OF DRIVEN
     +                    GAS'
        READ(*,30) MM4
        READ(*,30) MM1
        WRITE(*,*) 'INPUT DRIVING TUBE LENGTH,DRIVEN TUBE LENGTH'
        READ(*,30) X4
        READ(*,30) X1

-------------------------------------------------------------
C      ITERATIVE ROUTINE FOR CALCULATING THE INCIDENT SHOCK MACH
      NUMBER

C-------------------------------------------------------------
      M=1.11
        DO 50 I=1,100000
        E=((2*G1*(M**2))-(G1-1))/(G1+1)
        F=((G4-1)/(G1+1))*SQRT((G1*T1*MM4)/(G4*T4*MM1))
        G=M-(1/M)
        H=-((2*G4)/(G4-1))
        A=E*((1-F*G)**H)
        PRATIO=P4/P1
        B=PRATIO-A
        C=0.001
        IF(B .LE. C)GOTO 60
```

```
      M=M+0.00005
50    CONTINUE
C60   M=M(I)
60    WRITE(*,*) M ,I
C-----------------------------------------------------------------

C                    CALCULATION OF THE GAS PROPERTIES

C-----------------------------------------------------------------
      P2=P1*(((2*G1*M**2)-(G1-1))/(G1+1))
      E=(P2/P1)
      F=((G1+1)*(M**2))/(((G1-1)*M**2)+2)
      B1=(((G1*M**2-((G1-1)/2))*(((G1-1)/2)*M**2)+1))
     $     /((((G1+1)**2)/4)*(M**2)))
      WRITE(*,*) B1
      T2=300.00*B1
      G=(T2/T1)
      A1=SQRT(G1*(8314/MM1)*T1)
      B4=((((G1+1)/(G1-1))+2-(1/E))/(1+(((G1+1)/(G1-1))*(1/E))))
      P5=B4*P2
      WRITE(*,*) B4,P5
      H=(P5/P2)
      B2=H*(((G1+1)/(G1-1))+H)/(1+(((G1+1)/(G1-1))*H))
      T5=T2*B2
      WS=M*A1
      WR=WS*(2+((2/(G1-1))*(1/E)))/(((G1+1)/(G1-1))-(1/E))
      M3=(2/(G4-1))*(((E*(1/PRATIO))**((1-G4)/(2*G4)))-1)
      V2=(2*A1*((M**2)-1))/(M*(G1+1))
      NOMTIM=(X1/WS)*((WS-V2)/(WR+V2))
      RUNTIM=2*NOMTIM*1000
C-----------------------------------------------------------------
                              RESULTS

C-----------------------------------------------------------------
     WRITE(1,*) 'INPUT PARAMETERS '
      WRITE(1,80) P4
80    FORMAT(2X,'DRIVING PRESSURE  P4(psi) =  ',F10.5)
      WRITE(1,90) P1
90    FORMAT(2X,'DRIVEN GAS PRESSURE  P1(psi) = ',F10.5)
      WRITE(1,100) T4
100   FORMAT(2X,'DRIVING GAS TEMP  T4(K) = ',F10.5)
      WRITE(1,110) T1
110   FORMAT(2X,'DRIVEN GAS TEMP  T1(K) = ',F10.5)
      WRITE(1,120) X4
120   FORMAT(2X,'DRIVING SECTION LENGTH = ',F10.5)
      WRITE(1,130) X1
130   FORMAT(2X,'DRIVEN SEC LENGTH = ',F10.5)
      WRITE(1,*) 'SHOCK RESULTS'
      WRITE(1,140) P2
140   FORMAT(2X,'PRESSURE BEHIND INCIDENT SHOCK P2(psi) = ',F10.7)
      WRITE(1,150) T2
150   FORMAT(2X,'TEMP BEHIND INCIDENT SHOCK  T2(K)= ', F10.5)
      WRITE(1,160) M
160   FORMAT(2X,'SHOCK MACH # M = ',F10.7)
```

```
      WRITE(1,280) WS
280   FORMAT(2X,'INCIDENT SHOCK SPEED = ',F10.5)
      WRITE(1,*) 'PROPERTIES IN ZONE 3: TRAILING EXPANSION '
      V3=V2
      A3=(V3/M3)
      T3=(A3**2)/(G4*(8314/MM4))
      P3=P2
      WRITE(1,170) T3
170   FORMAT(2X,'TEMP IN ZONE 3, T3(K) = ',F10.5)
      WRITE(1,180) P3
180   FORMAT(2X,'PRESSURE IN ZONE 3, P3(psi) = ',F10.7)
      WRITE(1,190) A3
190   FORMAT(2X,'SOUND SPEED IN ZONE 3 , A3 = ',F10.5)
      WRITE(1,200) M3
200   FORMAT(2X,'M3 = ',F10.7)
      WRITE(1,210) P5
210      FORMAT(2X,'PRESSURE  BEHIND  REFLECTED  SHOCK  P5(psi)  =
     +    ',F10.5)
      WRITE(1,220) T5
220   FORMAT(2X,'TEMP BEHIND REFLECTED SHOCK  T5(K) = ',F10.5)
      WRITE(1,230) WR
230   FORMAT(2X,'REFLECTED SHOCK SPEED  WR(m/s) = ',F10.5)
      WRITE(1,*) 'TEST TIMES'
      WRITE(1,290) RUNTIM
290   FORMAT(2X,' RUNTIME IN MILLISEC, TIM(msec) =',F10.5)
      STOP
      END
```

```
C*****************************************************************
      Program To Calculate The Smoothened Data Points From The
      Measured Data Using First Order 3 Point Formula.  The Program
      Also Calculates The Temperature Derivatives Using Lagrange 5
      Point Formula.
C*****************************************************************
       DIMENSION Y(3000),T(3000),D(3000),A(3000),TEMP(3000)
       OPEN(1,FILE='B:\YAGNA\SHOCKTUN\STTHF12.ASC')
       OPEN(2,FILE='C:\YAGNA\STTHF8.OUT')
       OPEN(3,FILE='C:\YAGNA\DERIVT8.OUT')
       OPEN(8,FILE='C:\YAGNA\TEMP8.OUT')
       DO 10 I=1,2048
       READ(1,*) Y(I)
       T(I)=(((Y(I)-Y(1))*1000)/0.04)+293
       WRITE(2,*) T(I)
 10    CONTINUE
C      DO 30 J=1,2
       DO 40 K=1,2030
       D(K)=(((5*T(K))+(2*T(K+5))-(T(K+10)))/6.0)
       D(K+5)=(((T(K))+(T(K+5))+(T(K+10)))/3.0)
       D(K+10)=(((-T(K))+(2*T(K+5))+(5*T(K+10)))/6.0)
C      D(K+3)=0.1*((4*T(K+4))+(3*T(K+3))+(2*T(K+2))+(T(K+1)))
C      D(K+4)=0.2*((3*T(K+4))+(2*T(K+3))+(T(K+2))-(T(K)))
       T(K)=D(K)
       T(K+5)=D(K+5)
       T(K+10)=D(K+10)
C      T(K+3)=D(K+3)
C      T(K+4)=D(K+4)
C      WRITE(*,*) T(K)
C      WRITE(*,*) T(K+1)
C      WRITE(*,*) T(K+2)
 40    CONTINUE
C30    CONTINUE
       DO 100 L=1,2040
       WRITE(8,*) T(L)
 100    CONTINUE
       DO 60 M=103,122
       H=7*(0.0195263)
       A(M+16)=((1/(12*H))*((T(M))-(8*T(M+8))+(8*T(M+24))-
     +         (T(M+32))))
 60    CONTINUE
       DO 70 N=103,138
       WRITE(3,*) A(N)
 70     CONTINUE
       END
```

The vita has been removed from the scanned document